IEEE Access
Multidisciplinary | Rapid Review | Open Access Journal

Received 2 August 2023, accepted 20 August 2023, date of publication 25 August 2023, date of current version 6 September 2023.

Digital Object Identifier 10.1109/ACCESS.2023.3308825

RESEARCH ARTICLE

Performance Analysis of Student Psychology-Based Optimization for the Frequency Control of Hybrid-Power System

SOMNATH GANGULY[1], JOYTI MUDI[1], VIVEKANANDA MUKHERJEE[2], TAPAS SI[3], (Member, IEEE), SAURAV MALLIK[4], (Member, IEEE), AIMIN LI[5], AMAL AL-RASHEED[6], MOHAMED ABBAS[7], AND AYMAN ABDULHAMMED[8]

[1]Department of Electrical Engineering, Bankura Unnayani Institute of Engineering, Bankura, West Bengal 722146, India
[2]Department of Electrical Engineering, Indian Institute Technology (Indian School of Mines), Dhanbad, Jharkhand 826004, India
[3]Department of Computer Science and Engineering, University of Engineering and Management, Jaipur, Rajasthan 303807, India
[4]Department of Environmental Epigenetics, Harvard T. H. Chan School of Public Health, Boston, MA 02115, USA
[5]School of Computer Science and Engineering, Xi'an University of Technology, Xi'an, Shaanxi 710049, China
[6]Department of Information Systems, College of Computer and Information Sciences, Princess Nourah bint Abdulrahman University (PNU), P.O. Box 84428, Riyadh 11671, Saudi Arabia
[7]Department of Electrical Engineering, College of Engineering, King Khalid University, Abha 61421, Saudi Arabia
[8]Department of Biochemistry and Hormone, King Fahad Central Hospital, Gizan 82666, Saudi Arabia

Corresponding authors: Somnath Ganguly (somnath_aec82@yahoo.co.in), Saurav Mallik (sauravmtech2@gmail.com), and Amal Al-Rasheed (aaalrasheed@pnu.edu.sa)

This work was supported in part by the Princess Nourah bint Abdulrahman University Researchers Supporting Project, Princess Nourah bint Abdulrahman University, Riyadh, Saudi Arabia, under Grant PNURSP2023R235; and in part by King Khalid University (KKU), Abha, Saudi Arabia, through the Deanship of Scientific Research, under Grant R.G.P.1/302/44.

ABSTRACT Access to reliable electricity is crucial for rural development and improving the quality of life in remote areas. Standalone photovoltaic PV systems and hybrid power systems HPS are promising solutions for rural electrification. However, frequency stabilization is a critical challenge in such systems, and conventional control techniques are inadequate. This work proposes a novel approach to optimize the PID controller gains for the standalone PV-based isolated HPS (IHPS). The student psychology-based optimization algorithm (SPBOA) and quasi-oppositional-based whale optimization algorithm (QOWOA) are employed to enhance the performance of the IHPS models separately. The objective function considered is the integral of time absolute error (ITAE), and the frequency response profile is studied in the presence of the proposed SPBOA and QOWOA-based PID controllers. The results show that the proposed SPBOA outperforms the QOWOA in terms of reducing the ITAE by nearly 5% and minimizing the peak and settling time of the frequency response by 5%-7% in different scenarios. The transient responses of the systems to different input conditions are also analyzed, indicating that both the IHPS-I and IHPS-II models are feasible for remote rural electrification. Overall, the proposed approach offers an efficient solution to optimize the PID controller gains for frequency stabilization in standalone PV and HPS. The results demonstrate the benefits of using the SPBOA and QOWOA algorithms to enhance the performance of the systems, making them suitable for remote rural electrification.

INDEX TERMS Diesel engine generator, isolated hybrid power system, photovoltaic, proportional-integral-derivative, wind turbine generator, quasi-oppositional-based whale optimization algorithm, student psychology-based optimization algorithm.

LIST OF ABBREVIATIONS

DEG	Diesel engine generator.
FOD	Figure of demerit.
GHPS	Grid connected hybrid power system.
HPS	Hybrid power system.
DEG	Diesel engine generator.
IAE	Integral of absolute error.
IHPS	Isolated hybrid power system.
ISE	Integral of square error.

The associate editor coordinating the review of this manuscript and approving it for publication was Shiwei Xia.

ITAE	Integral of time multiplied absolute error.
ITSE	Integral of time multiplied squared error.
LFC	Load frequency control.
MPP	Maximum power point.
MPPT	Maximum power point tracking.
OBL	Opposition based learning.
PD	Proportional-derivative.
PI	Proportional-integral.
PID	Proportional-integral-derivative.
SPV	Solar photovoltaic.
PUGs	Power generation units.
PWM	Pulse-width modulation.
QOBL	Quasi-oppositional based learning.
QOWOA	Quasi-oppositional based whale optimization algorithm.
RESs	Renewable energy sources.
RLP	Random load perturbation.
RSLP	Random SLP.
SLP	Step load perturbation.
STC	Standard test conditions.
STPP	Steam turbine power plant.
SPBOA	Student psychology-based optimization algorithm.
WOA	Whale optimization algorithm.
WTG	Wind turbine generator.

I. INTRODUCTION

A. GENERAL

Owing to the increased civilization and industrialization of developed and emerging countries, there is a growing interest in power. Still, in the twenty-first century, the portfolio of electrical power generation is heavily dependent on fossil fuels. As a result, fossil fuels are severely depleted, and our living ecosystem is increasingly contaminated and degraded. Worries about environmental change have coordinated towards the development of renewable energy sources (RESs) based power generation. The RESs (like photo-voltaic (PV) cells, wind energy, hydro, tidal, geothermal, and solar thermal energy) are playing an important role in power generation by integrating these models to create hybrid power systems (HPSs). HPS are facing the challenge of integrating renewable energy sources into the power mix, but they are overcoming this challenge through advanced control systems, energy storage, and flexible designs. As renewable energy technologies continue to improve, hybrid power systems will play an increasingly important role in meeting our energy needs in a sustainable and efficient way.

Among the RESs, PV [1] and wind turbine generators (WTGs) [2] are the most promising and popular power generation units (PUGs) that produce green and clean electricity. In this regard, the conventional power-generating units may be improved in terms of their quality and reliability if the RESs are added. The electrification of rural areas is difficult and expensive to integrate with the national grid because of their remote location and lower power demand. Especially in these areas, RES-based isolated HPS may be deployed more quickly and economically [3], [4]

B. LITERATURE SURVEY

Day by day, electricity demand and environmental pollution are increasing in parallel. The burning of fossil fuels pollutes the surrounding area with the emission of smoke and dust. In this case, the RESs are incorporated into conventional power-generating units. The output RESs are intermittent, resulting in a fluctuation in output power and frequency. To resolve these concerns, the concept of independent power generation may control the power and the frequency for rural, medium, and small industries. In an isolated power system, diesel engine generators (DEGs) are the main sources of power. The DEGs are connected with WTGs, making an isolated HPS (IHPS) [5]. However, the IHPS model is capable of controlling load frequency within a limited range of load and wind disturbance [6]. The voltage fluctuations occur due to the difference between reactive power generation and consumption at the WTG terminal, which decreases the IHPSs' stability and reliability [7]. In IHPS, the DEG pollutes the environment through the emission of smock. For that reason, solar power (PV cells connected in a string) has been connected with IHPS to generate green power. PV and WTG are the most promising RESs that are being employed for the benefit of the environment [8]. Moreover, many countries have taken the initiative to increase power generation from solar PV and WTGs as solar PV subsidies have been imposed on customers.

In standalone IHPS, integration of solar PV and WTGs is the most important and manageable RES [9], as it may improve quality and reliability compared to single resources. WTG, PV, and hydroelectric power plans have been discussed in the context of modeling, control, and operation [10]. Isolated and grid-tied solar power plants have been connected with DEGs and batteries [11]. This is a sustainable, economically viable, and environmentally friendly HPS for the desalination plant. This study incorporates solar PV, WTGs, biomass, and vanadium redox flow batteries into a micro-grid designed and implemented in [12]. Automatic generation control of a more realistic two-area multi-source power system with hydro, thermal, gas, and wind energy plants in each control area [13]. In [14] and [15] the investigated standalone micro-grid system included a PV system, a WTG, and a DEG as distributed energy sources. However, in the standalone IHPS, the maximum power point (MPP) tracking (MPPT) approach is utilized to get the optimum output of the electric power [16].

RES generation is inherently unpredictable and is dependent on current climate conditions and might affect the output of the IHPS. A feedback controller controls the DEG's governor speed, WTG's pitch angle, and the MPPT technique for solar PV modules to attain the optimum quality power and frequency of IHPS. The most common technique for controlling the IHPS is the use of classical controllers (such as

fixed-gain proportional-integral (PI), proportional-derivative (PD), and proportional-integral-derivative (PID) controllers). The enormous application of the PID controller in power and process industries is due to its simplicity in design and having fewer parameters to tune. In [17] a fractional-order proportional derivative - cascade controller as a novel control structure to improve the execution of automatic generation control for the load flow management of an interconnected power system.

Different optimization algorithms have been implemented in IHPS-I and II to enhance the performance of the controllers and tune the gain parameters with or after changes in load demand. A genetic algorithm, particle swarm optimization, and mine blast algorithm are applied in [18] to a hybrid power system model to control the output power and frequency. The bio-geography-based optimization algorithm has been utilized to optimize the PID controller gain parameters in [19]. In [20], PI and PID controllers have been tuned by using differential evolution to improve the frequency deviation profiles of a hybrid multi-area power system, which is a combination of renewable and non-renewable-based energy resources. The firefly algorithm has been used in [21] to tune the PI controller for the load frequency control (LFC) of a system consisting of a PV system and a thermal generator. In [22] and [23], the Salp Swarm Algorithm is used to fine-tune the PID controller parameters for multi-area LFC.

The LFC-based adaptive control implemented in large multi-interconnected systems was designed using multi-verse optimization [24]. The Moth flame optimization technique [25] has been applied in the HPS model to tune the parameters of the controller gains and energy storage devices. The automatic generation and control of the LFC are categorized into two main phases: primary frequency control and secondary control [26]. It provides an in-depth analysis of the power system operation challenges presented by the significant deployment of PV sources. The Harris Hawks Optimizer [27] was implemented for tuning the parameters of a PI-based LFC, incorporated into a multi-interconnected system with RESs. The Wrapper-based deep feature optimization algorithm, Mimetic algorithm, and harmonic search algorithms, which are used to solve large and complex problems have been used in [28] and [29].

C. MOTIVATION

This paper analyses and studies the IHPS-I and IHPS-II models. For the IHPS-I model, power-generating units such as DEG, WTG, and solar PV (SPV) are considered. The IHPS-II consists of one WTG and one steam turbine power plant (STPP). According to the existing literature, the majority of researchers are focused on HPS, which is a combination of WTG and DEG or WTG, solar PV, and biomass. Reference [30] takes into account a 40 kWp solar PV power plant (connected via MPPT and boost converter), a 150 kW DEG, and a 150 kW WTG. However, much more investigation should be carried out in the presence of step load perturbation demand, where in real-time, the load demand and wind velocity change continuously. Nevertheless, the magnitude of load demands never crosses the pre-defined limits. The missing context of discontinuous change in demand for load and wind velocity is explored in the studied IHPS model in the present work. In these circumstances, the frequency deviation profile is affected. So, the frequency response of the IHPS model (*i.e.*, overshoot, undershoot, rise time, and steady-state error) needs to be analyzed. A novel index is introduced in [31], [32], and [33] that evaluates changes in two indicators of frequency deviation and frequency response of inertia during a specific period following a disturbance. This index has the ability to quickly detect system instability and simultaneously provide a timely estimation of voltage instability in power systems.

In the next phase of the literature survey, problems associated with the tuning methodologies of the controller used in IHPS-I and II models are vividly analyzed and discussed. To handle these challenges, the researchers have designed different types of control techniques. An optimization technique is adopted for optimizing the controller's parameters which improves the frequency deviation profile of the considered models. During this evolution of optimization techniques, researchers have found lots of limitations and problems. The researchers are aiming to improve existing optimization algorithms while also seeking novel optimization algorithms to address complicated engineering issues efficiently and fast.

The new optimization technique, the student psychology-based optimization algorithm (SPBOA), has been found to be extremely effective in finding the correct value of variables from a large search area [34]. The proposed SPBOA is being used in the area of load frequency control of HPS [35], [36], [37]. The whale optimization algorithm (WOA) is a new population-based optimization method, a metaheuristic optimization algorithm inspired by nature [38]. This mimics the humpback whales' social behavior. The pioneering theory of opposition-based learning (OBL) was initiated in 2005 [39]. The partial centroid opposition-based learning a novel Opposition-based scheme has been applied in [40]. It aids in accelerating the convergence of various optimization methods. Then, a concept of population initialization has been implemented after OBL (such as quasi-oppositional based learning (QOBL)) in [41]. In this work, the idea of QOBL has been incorporated with WOA in the initialization phase. In this research, the notion of QOBL was employed to improve the convergence rate of fundamental WOA. As a result, this paper's approach has been dubbed quasi-oppositional based WOA (QOWOA) [42].

D. CONTRIBUTION OF THE PRESENT WORK

In light of the discussion carried out in the preceding subsections, this paper's main contributions are as follows:

(a) In this paper, a cutting-edge IHPS-I model (incorporating DEG, WTG, and solar PV) is designed and developed, which may aid in improving electricity demand in

urban and suburban areas and eradicating the electricity deficit.

(b) The modeling of IHPS-II (a combination of one WTG, solar PV (from the RES group), and one STPP (a very common type of non-RES) is carried out for uninterrupted power supply to the rural population.

(c) A PID controller is incorporated into the proposed model for further frequency control intervention.

(d) The SPBOA and QOWOA, as optimization tools for the studied IHPS-I and IHPS-II models, are explored.

(e) The proposed SPBOA and QOWOA technique is studied for two adopted models, to find the optimized parameter values of the PID controllers deployed.

(f) To cope with more real-world designs, the frequency responses of tested models are presented for different cases of load and wind uncertainty.

(g) The frequency responses of the SPBOA and QOWOA systems are demonstrated in this work.

The article's strength lies in its detailed investigation of LFC in renewable energy-based power systems for remote electrification, highlighting the challenges of insufficient energy supply, unreliable sources, and lack of storage, as well as the need for innovative solutions, policies, and limited resources. The artificial intelligence-based design of hybrid power systems *i.e.*, the application of two Swarm Intelligent (SI) algorithms in frequency stabilization, and the analysis of various uncertainties add important values to this study. This study aims to optimize the control of an IHPS by analyzing the impact of uncertainties on load demand and wind perturbation inputs. This research is focused on reducing greenhouse gas emissions and combating climate change.

E. LAYOUT OF THE PAPER

In the following sections, the rest of the paper is reported. *Section II* studies the basic design and components of IHPS-I and II. The problem formation associated with the studied IHPS-I and II models is described in *Section III*. *Section IV* presented a short overview of the proposed algorithm. In *Section V*, it puts emphasis on simulation-based performance study and analysis. Finally, *Section VI* summarizes the final observations while indicating some future work scopes.

II. SYSTEM MODELING

A. ADAPTED IHPS-I MODEL

The adapted IHPS-I comprises a WTG of 150 kW, a DEG of 150 kW, and a solar PV of 40 kWp [42]. Fig. 2 depicts the schematic model of the tested IHPS-I system. The model's parameters are presented in Table 7 of the Appendix Section. The power balance equation of the IHPS-I model is presented in eq. (1) (see Fig. 2).

$$\Delta P_{IHPS-I} = \Delta P_{GD} + \Delta P_{PV} + \Delta P_{GW} - \Delta P_L \quad (1)$$

where, ΔP_{IHPS}, signifies the IHPS output power deviation, ΔP_{GD}, shows the change in the output power of DEG's, ΔP_{GW}, signifies the change in the output power of WTG,

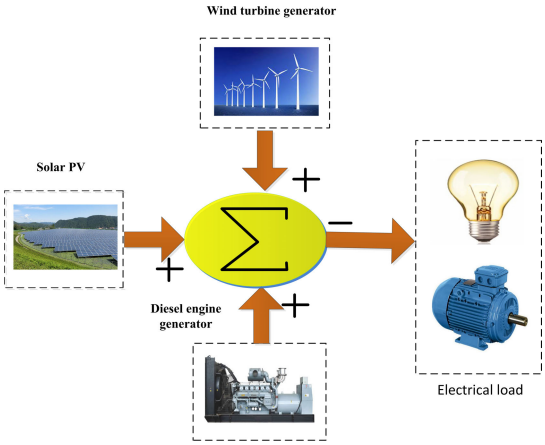

FIGURE 1. Schematic model configuration model of the studied IHPS-I.

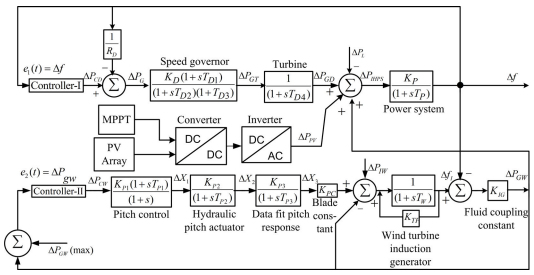

FIGURE 2. Linear transfer function model of the studied IHPS-I.

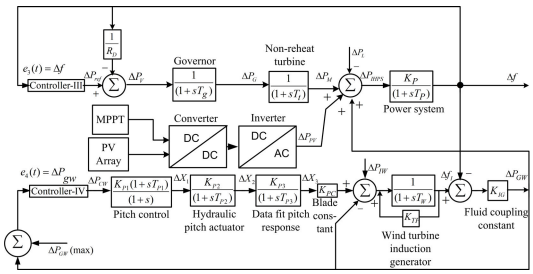

FIGURE 3. Block diagram representation of the studied IHPS-II.

ΔP_{PV} shows the solar PV's output power deviation and ΔP_L, signifies the load deviation.

B. ADAPTED IHPS-II MODEL

The IHPS-II configuration is shown in Fig. 3. For this model, the net power equation is presented in (2).

$$\Delta P_{IHPS-II} = \Delta P_{GW} + \Delta P_M + \Delta P_{PV} - \Delta P_L \quad (2)$$

In (2), $\Delta P_{IHPS-II}$, signifies the IHPS-II output power deviation, ΔP_{GW}, signifies the WTG's output power deviation, ΔP_M, signifies the STPP's output power deviation and, ΔP_{PV}, is the solar PV's output power deviation.

C. REPRESENTATION OF THE PGUs

1) BASIC CONCEPT OF DEG

The dynamic model of the DEG is shown in Fig. 2 [43]. The equations of the transfer function are shown in (3)-(5).

$$\Delta P_{GD} = \left(\frac{1}{1 + sT_{D4}}\right) \Delta P_{GT} \quad (3)$$

$$\Delta P_{GT} = \left(\frac{K_D\,(1+sT_{D1})}{(1+sT_{D2})\,(1+sT_{D3})}\right)\Delta P_G \tag{4}$$

$$\Delta P_G = \Delta P_{CD} - \left(\frac{1}{R_D}\right)\Delta f \tag{5}$$

where ΔP_G is the speed governor(SG) input signal in p.u.,ΔP_{GT} is the DEG input signal in p.u., ΔP_{CD} is the SG input signal in p.u., K_D signifies the governor gain, R_D signifies the SG regulation in Hz/p.u.,T_{D1}, T_{D2} and T_{D3} are the SG time constants in sec, T_{D4} is the time constant of the turbine in sec and Δf signifies frequency deviation in p.u.

D. WTG FUNDAMENTAL CONCEPT

The wind energy system transforms mechanical energy into electrical energy by converting the kinetic energy of moving air. The power output from the wind turbine (P_t) is presented in (6)

$$P_t = \frac{1}{2}C_p\,(\lambda,\beta)\,\rho\pi R^2 v^3 \tag{6}$$

where ρ signifies the density of air, R signifies the blade radius, β, signifies the angle of the pitch, λ, implies the tip speed ratio, v, implies the linear wind velocity and C_p signifies the power coefficient. Fig. 2 depicts the WTG dynamic model.

As stated in (7), the fluid coupling block converts the difference in speed of the generator and turbine frequency to electricity [43].

$$\Delta P_{GW} = K_{IG}[\Delta f_I - \Delta f] \tag{7}$$

where, P_{GW} denotes the output power deviation, K_{IG} is the fluid coupling gain and Δf_I is the speed deviation of the WTG.

The wind turbine induction generator (WTIG) speed is shown in equation (8).

$$\Delta f_I = \left(\frac{1}{1+sT_W}\right)[K_{TP}\Delta f_I - \Delta P_{GW} + K_{PC}\Delta X_3 + \Delta P_{IW}] \tag{8}$$

where Δf_I is the speed deviation (refer to frequency deviation) in p.u. of the WTIG, K_{PC} is the gain of blade characteristic,P_{IW} is the input of wind power deviation in p.u., ΔX_3 is the output of the data fit pitch response.

The data fit pitch response block is functioning here as a basic lag compensator that matches the model gain characteristic. The output is represented in equation (9).

$$\Delta X_3 = \Delta X_2\left[\frac{K_{P3}}{1+sT_{P3}}\right] \tag{9}$$

where ΔX_2 is the hydraulic pitch actuator output, K_{P3} is the block gain of the data fit pitch,and T_{P3} is the time constant of data fit pitch response in sec.

The pitch angle of the turbine is controlled by the hydraulic pitch actuator. The performance is represented in equation (10).

$$\Delta X_2 = \Delta X_1\left[\frac{K_{P2}}{1+sT_{P2}}\right] \tag{10}$$

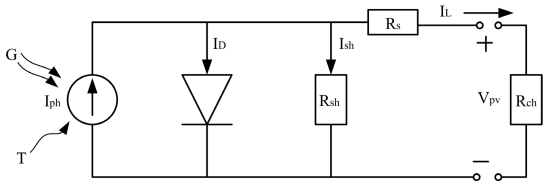

FIGURE 4. Equivalent circuit of the SPV cell.

where ΔX_1 is the pitch controller output, X_2 is the gain of the hydraulic pitch actuator, and T_{P2} is the time constant of the hydraulic pitch actuator in sec.

The WTG's pitch angle is selected precisely to get the turbine's maximum output power. In Fig. 2, it is possible to define the value of ΔX_1 by (11).

$$\Delta X_1 = \Delta P_{CW}\left[\frac{K_{P1}\,(1+sT_{P1})}{1+s}\right] \tag{11}$$

where ΔP_{CW} is the control signal of the pitch control block in p.u., K_{P1} is the gain of the pitch control block, and T_{P1} is the time constant of the pitch control block in sec.

1) SOLAR PV: FUNDAMENTALS

Solar PV is one of the most reliable and clean energy resources that convert sunlight into electricity. Fig. 4 shows the circuit diagram of the solar PV model [44]. The load current (I_L) of the PV cell under normal conditions is given in (12).

$$I_L = I_{ph} - I_d - I_{sh} \tag{12}$$

where I_{ph} is the SPV module's photocurrent, depending on irradiance and temperature, the current across the diode is considered as I_D and I_{sh} is the current of the shunt resistor (R_{sh}).

The photocurrent of SPV can be expressed as in (13).

$$I_{ph} = I_{sc}\left(1 - K_1\left(exp\left(K_2.V_{mpv} - 1\right)\right)\right) \tag{13}$$

where, K_1, K_2 and m are the coefficients. The value of coefficient K_1 is taken as 0.01175 and the other two are in sequence, represented by (14) - (15).

$$K_2 = \frac{K_4}{V_{oc}^m} \tag{14}$$

$$m = \frac{ln\left[\frac{K_3}{K_4}\right]}{ln\left[\frac{V_{mpp}}{V_{oc}}\right]} \tag{15}$$

In (14), the values of K_3 and K_4 are, in order, represented by (16) and (17).

$$K_3 = ln\left[\frac{I_{sc}\,(1+K_1) - I_{mpp}}{K_1 * I_{sc}}\right] \tag{16}$$

$$K_4 = ln\left[\frac{1+K_1}{K_1}\right] \tag{17}$$

where K_4 and V_{oc} represent the coefficient and open-circuit voltage of the terminal, respectively, I_{sc} is the short circuit current and I_{mpp} is the maximum power point current in ampere, V_{oc} and V_{mpp} are the open-circuit voltage and the

maximum power point voltage in the terminal of SPV module, respectively. and $K_1 = 0.01175$.

When the temperature increases, the solar panel's production of power gradually decreases. Due to the effect of temperature, the following parameters change in solar PV modules in accordance with (18) - (20).

$$\Delta T_c = T_c - T_{stc} \tag{18}$$

$$\Delta I_L = \alpha_{sc}\left(\frac{G}{G_{stc}}\right)\Delta T_c + \left(\frac{G}{G_{stc}} - 1\right) I_{sc,stc} \tag{19}$$

$$\Delta V_{pv} = -\beta_{oc}\Delta T_c - R_s \Delta I_L \tag{20}$$

where ΔT_c is the change in the temperature, $T_c$is the cell temperature, and T_{stc} is the temperature at standard test conditions (STC) 25^0C, $I_{sc,stc}$ is the short circuit current at STC of a solar PV module,G is the solar irradiation and $G_{stc} = 1000W/m^2$, temperature coefficient, ΔV_{pv} is the change in the voltage, β_{oc} is the open circuit temperature coefficient, R_s and ΔI_L is the resistance and change in the load current respectively. The parameters of the Canadian solar (Model type: CS3U-350P) which have been used in this study are represented in Table 8.

2) THE FUNDAMENTAL CONCEPT OF MPPT TECHNIQUE

The MPPT algorithm is necessary for the improvement of the effectiveness of the solar PV module. The nature of the irradiance and the temperature are always nonlinear. For that reason, the output power of solar PV is never constant. However, when the MPPT algorithm is incorporated with solar PV, the system always runs at maximum output. The maximum power output of a solar PV module depends upon three major factors. These are irradiance, cell temperature, and load impedance. Different techniques have been used in the open literature for MPPT, such as fractional open circuit, fractional short circuit, perturb and observe [45], incremental conductance (IC) [46] etc. Among these methods, the IC technique was adopted in this study. This method tracks the MPP from the P-V curve of the solar PV when $\frac{dI_L}{dV_{pv}} = 0$ At this point, the duty (D) is fixed. It is positive when the output voltage (V_{pv}) is less than the MPP voltage and negative when the V_{pv} is greater than the MPP voltage. The following mathematical equations (see (21-24)) may be derived for the IC technique.

$$\frac{dP}{dV} = \frac{d(V_{pv}.I_L)}{dV_{pv}} = I_L + V_{pv}\frac{dI_L}{dV_{pv}} = 0 \tag{21}$$

$$\frac{\Delta I_L}{\Delta V_{pv}} = -\frac{I_L}{V_{pv}} \Rightarrow MPP \tag{22}$$

$$\frac{\Delta I_L}{\Delta V_{pv}} > -\frac{I_L}{V_{pv}} \Rightarrow left\ of MPP \tag{23}$$

$$\frac{\Delta I_L}{\Delta V_{pv}} < -\frac{I_L}{V_{pv}} \Rightarrow right\ of MPP \tag{24}$$

3) DC-DC CONVERTER: PRINCIPLE OF OPERATION

In this study, the boost converter (shown in Fig.5) is considered in the MPPT system [47]. During the ON stage of the

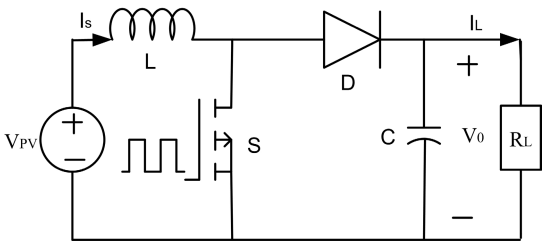

FIGURE 5. DC-DC boost converter.

MOSFET, $T_{ON} > t. > 0$. At that time, the diode is reverse-biased, and the current flows through the inductor (L). During $T_{ON} > t > T$, the MOSFET is in the OFF state and the diode becomes forward-biased. The time period is defined by (25)

$$T = T_{ON} + T_{OFF} \tag{25}$$

where T_{ON} and T_{OFF} are, in order, ON and OFF time of the MOSFET.

The value of switching frequency ($f_{switching}$) is determine by(26).

$$f_{switching} = \frac{1}{T} \tag{26}$$

The value of duty cycle (D) is calculated by (27).

$$D = \frac{T_{ON}}{T} \tag{27}$$

During the ON state, the inductor current has a positive slope toward the highest value and then a negative slope back to the initial value at a steady state. Over the course of a complete cycle, the total charge of the inductor current is zero. The input voltage (V_{PV}) and the output voltage (V_0) of the converter are interrelated by eq. (28).

$$\frac{V_0}{V_{PV}} = \frac{1}{1-D} \tag{28}$$

The inductor (L) and capacitor (C) values are calculated by equations (29) and (30), respectively,

$$L = \frac{V_{PV}.(V_0 - V_{PV})}{\Delta I_L f_s.V_0} \tag{29}$$

$$C = \frac{I_L.D}{f_s.\Delta V_0} \tag{30}$$

where f_s is the switching frequency, ΔI_L is the ripple current of the inductor, ΔV_0 is the ripple voltage of the output and I_L is the load current.

4) DC-AC INVERTER: PRINCIPLE OF OPERATION

The inverter converts dc power to ac power at desired output voltage and frequency. The inverter can be classified into two types, voltage source, and current source inverter. Fig. 6 is shown the single-phase inverter in full bridge topology. The voltage equations are the following equations.

$$\frac{V_d}{2}(S_{11} - S_{12}) = V_{an} + V_{no} = V_{ao} \tag{31}$$

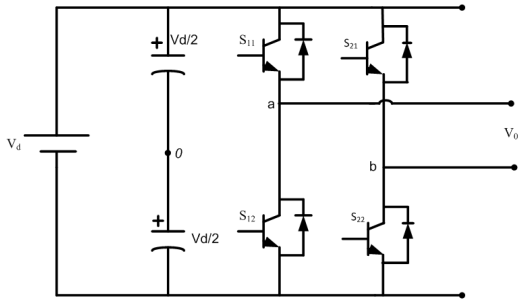

FIGURE 6. Schematic diagram of PWM inverter.

$$\frac{V_d}{2}(S_{21}-S_{22}) = V_{bn} + V_{no} = V_{bo} \tag{32}$$

$$V_{ab} = V_{an} - V_{bn} \tag{33}$$

The V_{an} and V_{bn} are the voltage of $a$and b phase to an arbitrary point n, *and* V_{no} is the voltage between n and the mid-point of the capacitor terminal. The switching operation of the inverter can be approximated by $\frac{1}{2}(1 + M)$, where M is the signal modulation signal.

$$M_{11} = \frac{2\,(V_{an}+V_{no})}{V_d} \tag{34}$$

$$M_{21} = \frac{2\,(V_{bn}+V_{no})}{V_d} \tag{35}$$

The switching operations of the inverter are S_{11}, S_{22}, and S_{21}, S_{12} turn on and turn off at the same time. The output voltage is determined by comparing the control signal, V_r, and triangular signal, $V_c$of the pulse-width modulation (PWM) which gives the switching pulses to the switches. The switching pattern of the inverter is as follows.

$$\begin{aligned} V_r > V_c, \quad & S_{11}\text{is on} \Rightarrow V_{ao} = \frac{V_d}{2} \\ \text{and} \quad & S_{22}\text{is on} \Rightarrow V_{bo} = -\frac{V_d}{2} \end{aligned} \tag{36}$$

$$\begin{aligned} V_r < V_c, \quad & S_{12}\text{is on} \Rightarrow V_{ao} = -\frac{V_d}{2} \\ \text{and} \quad & S_{21}\text{is on} \Rightarrow V_{bo} = \frac{V_d}{2} \end{aligned} \tag{37}$$

5) PID CONTROLLER

A PID controller is used here in this study for the stabilization of load frequency and for improving the system's dynamic response. The appropriate PID controller structure necessitates determining optimal values for its three parameters (*i.e.* proportional (K_p), integral (K_i) and derivative (K_d) gains) in a parallel structure to determine the optimum output (refer Fig. 7). The PID controller's control action is defined by the equation (38).

$$u(t) = K_p e(t) + K_i \int_0^t e(t)dt + K_d \frac{d}{dt}e(t) \tag{38}$$

where $u(t)$ and $e(t)$ are the actuating signal and the error signal, respectively. In (38), K_p, K_i, and K_d are, in order, proportional, integral, and derivative gain constants of the controller.

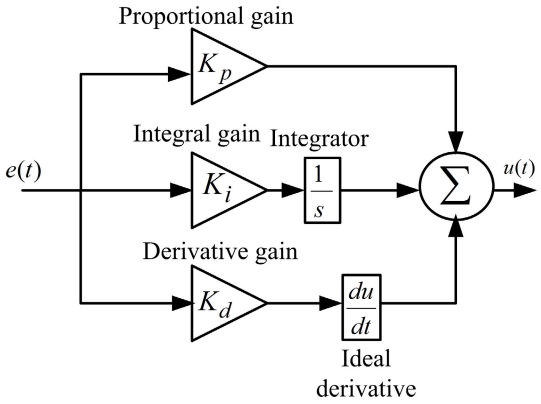

FIGURE 7. Structure of the PID controller.

The error inputs to the PID controllers for the IHPS-I and IHPS-II models are presented, in sequence, by (39) - (42) [42].

$$e_1(t) = \Delta f \tag{39}$$

$$e_2(t) = \Delta P_{GW} - \Delta P_{GW(\max)} = \Delta P_{gw} \tag{40}$$

$$e_3(t) = \Delta f \tag{41}$$

$$e_4(t) = \Delta P_{GW} - \Delta P_{GW(\max)} = \Delta P_{gw} \tag{42}$$

III. PROBLEM CONFIGURATIONS

A. PERFORMANCE INDICES OF THE SYSTEM

For the present study, the following performance indices have been considered for the studied IHPS-I and II models: integrated absolute error (IAE), integrated squared error (ISE), integrated time weight absolute error (ITAE), and integrated time weight square error (ITSE). The mathematical expressions for these indices with a simulation time of tare are given in the following order: (43) - (46).

$$IAE = \int_0^\alpha |\Delta f|dt \tag{43}$$

$$ISE = \int_0^\alpha |\Delta f|^2 dt \tag{44}$$

$$ITAE = J = \int_0^\alpha t|\Delta f|dt \tag{45}$$

$$ITSE = \int_0^\alpha t|\Delta f|^2 dt \tag{46}$$

B. DESIGN OF OBJECTIVE FUNCTION

ITAE serves as an objective function (J) for the methodology for optimizing this study. It's also known as a demerit figure

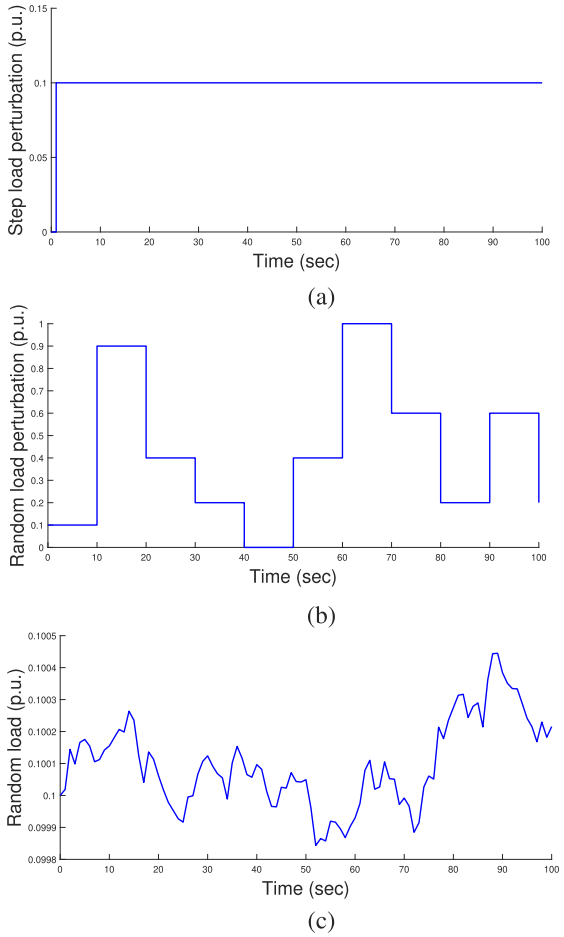

FIGURE 8. Profiles of different perturbations used (a) SLP, (b) RSLP, and (c) RLP.

(FOD). ITAE accords settle faster than ISE and ITSE equivalents. The maximum percentage of overshoot is also restricted as this absolute error is included in the ITAE criterion. When compared to other integral-based performance metrics, the ITAE produces better results [41]. It is preferred over other objective functions in certain situations because it is sensitive to the magnitude and duration of the error. This means that it gives a higher weight to errors that persist for a longer time.ITAE is useful in systems where it is more important to minimize the overall error than just the maximum error at any given instant. This study's mathematical problem can be expressed in (47).

$$Minimize\ J = Minimize\ ITAE \tag{47}$$

C. CONSTRAINTS OF THE OPTIMIZATION PROBLEM

The tunable parameters of the controller incorporated into the investigated IHPS-I and II models are exposed to a specific, limited range throughout the optimization process in the current optimization procedure. The gains of the PID controller are constrained by the limits indicated in (48).

$$\left.\begin{aligned} K_P^{\min} \le K_P \le K_P^{\max} \\ K_I^{\min} \le K_I \le K_I^{\max} \\ K_D^{\min} \le K_D \le K_D^{\max} \end{aligned}\right\} \tag{48}$$

D. TRANSIENT PARAMETER SPECIFICATION

The major objective of this article is to optimize the controller gain tuning parameters such that the power system dynamic response is not too fast or even too slow. The system's dynamic behavior is measured in terms of rise time (T_r), settling time (T_s), peak value (M_p), and peak time (T_p) calculated. The values of all the above-mentioned performance indices and transient performances are calculated at the completion of the program that has been developed.

IV. FORMULATION OF SPBOA AND QOWOA

A. WOA

The WOA is a nature-inspired metaheuristic optimization system that mimics humpback whale social behavior [48]. The humpback whale hunts using the strategy of bubble-netting near the water's surface. They dive their prey 12m below, and then catch them by swimming near the surface in a 9-shape path or in a spiral shape. In comparison to typical metaheuristic algorithms, the outcome of WOA is quite powerful [48], [49]. The WOA begins with a set of random individuals, who renew their positions after each iteration. The new position is with respect to either a randomly selected search agent or the best solution gained so far. The major steps of whale hunting are (a) encircling the prey, (b) bubble-net attacking (exploitation stage) and (c) searching for the prey (exploring stage). Considering the above-mentioned process of catching the prey. The WOA is formed and will be discussed below.

In terms of convergence speed and achieving an optimal solution, metaheuristic algorithms have both efficiency and limitations. The limitations of WOA are as follows:

(a) In the stage of exploitation and exploring, the search agent has chosen a randomization technique, which may take more time, specifically in the case of difficult engineering problems.

(b) The parameters chosen in the stage of encircling the prey are very important. Due to this factor, the convergence speed may be poor at the stage of exploration and exploitation [49].

(c) Within the search area, WOA employs the encircling mechanism, which is less capable of escaping from a locally optimal solution. As a result, poor performance occurs. It also has a drawback when it comes to optimizing the best solution after each cycle [50].

Due to the above limitations, to increase WOA's exploration potential, the QOBL [41] concept has been introduced. It employs a random number population with its quasi-opposite number in order to (a) improve performance, (b) avoid premature convergence, (c) increase solution diversity, and (d) accelerate the convergence speed of the basic

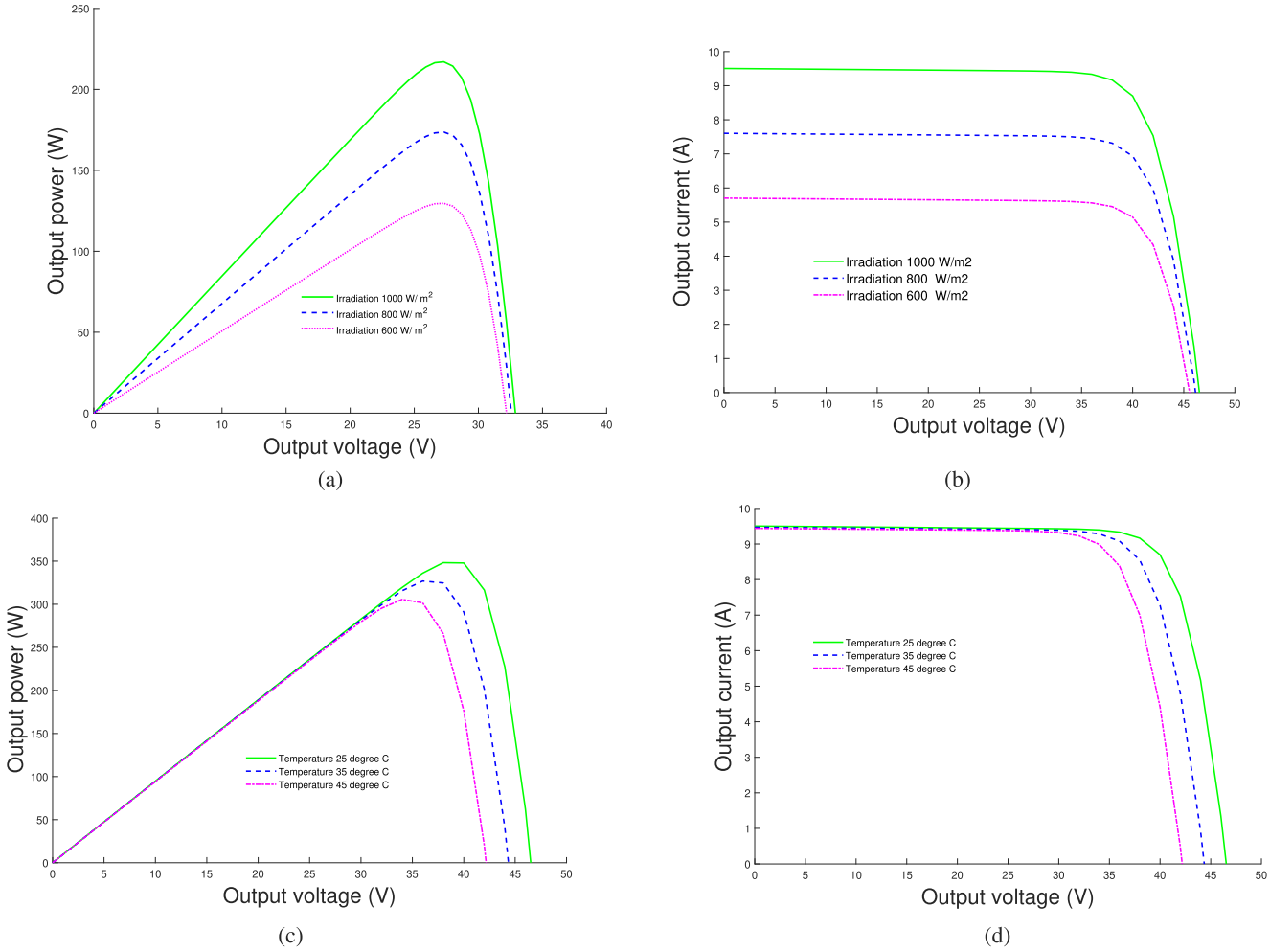

FIGURE 9. Characteristics of SPV (a) *P-V* curve *w.r.t.* irradiation, (b) *I-V* curve *w.r.t.* irradiation, (c) *P-V* curve *w.r.t.* temperature and (d) *I-V* curve *w.r.t.* temperature.

WOA. QOWOA has been used for HPS problems due to its increased exploring capability [42]. The flowchart of QOWOA is provided in Fig. 10.

B. SPBOA

SPBOA is a new concept [34] based on student psychology, in which students are constantly attempting to improve their academic performance by trying to compare themselves to their fellow students. Students in a classroom are divided into four groups: (a) the best students, (b) good students, (c) average students, and (d) students who strive to improve at random. The best student in the class is someone who gets the highest grade on the exam. In comparison to other students, this student has put in the most effort in all subjects offered in this batch. On the other hand, a student's performance is highly dependent on their effort and capability in their chosen subject. However, on the exam, not all students receive the same grade. It varies depending on the subject. It is determined by the student's psychological state. A good student is always striving to outperform the best student. At the same time, average students try to put in more effort than they had in the past, and some students try to improve their performance on a whim. Based on the preceding discussion, the SPBOA may take the following steps

Step 1: Set the optimization parameters and start the class's initial population.
Step 2: Retrieve the students' initial performance.
Step 3: Explore the student categories.
Step 4: Investigate the class's performance.
Step 5: Take note of the best solution.
Step 6: **Steps 3** and **5** ought to be repeated till the terminator requirements are met.

The flowchart of SPBOA is provided in Fig. 11. It is a relatively new optimization algorithm that draws inspiration from the behavior and decision-making processes of students. Here are some of the advantages of using SPBOA:

1) Fast convergence: SPBOA has demonstrated fast convergence rates in optimization problems compared to other algorithms, such as Genetic Algorithm and Particle Swarm Optimization.

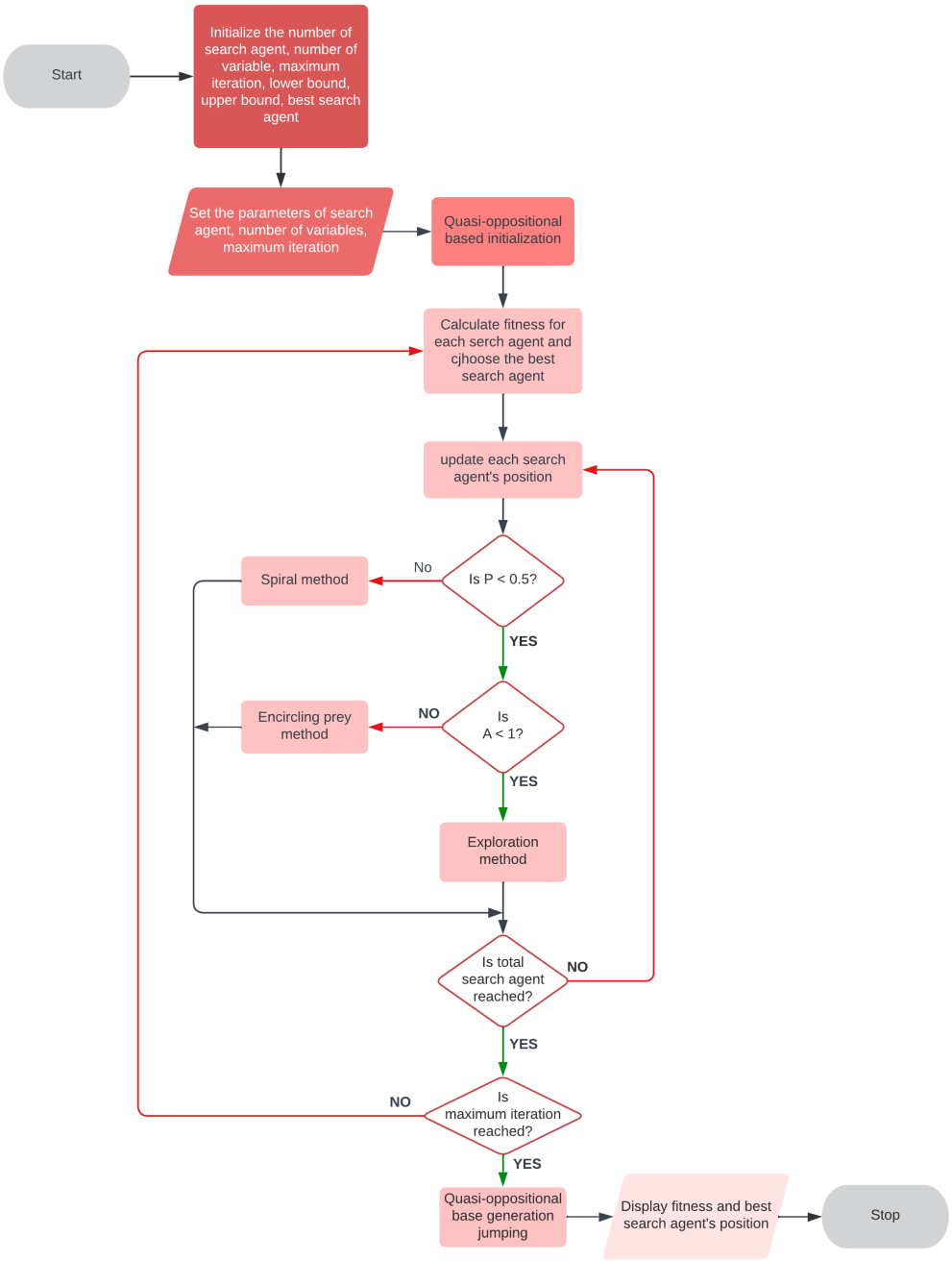

FIGURE 10. Flowchart of the QOWOA.

2) Robustness: SPBOA is robust to noise and can handle non-linear, non-convex, and high-dimensional optimization problems.
3) Low computational cost: SPBOA is computationally efficient and can handle large-scale optimization problems.
4) Global optimization: SPBOA is effective in finding global optima, which is particularly useful in complex optimization problems where finding the optimal solution is challenging.

V. RESULTS AND DISCUSSION

This study involves the simulation and analysis of two power system models under various operating conditions. The first model, IHPS-I, is comprised of three generating units (WTG, DEG, and solar PV), while the second model, IHPS-II, includes a WTG, solar PV, and an STPP. Controllers I and II are used to control the DEG governor and WTG pitch angle for IHPS-I, while Controllers III and IV are utilized for the STPP governor and WTG pitch in IHPS-II. The study applies the proposed SPBOA and QOWOA to tune the PID

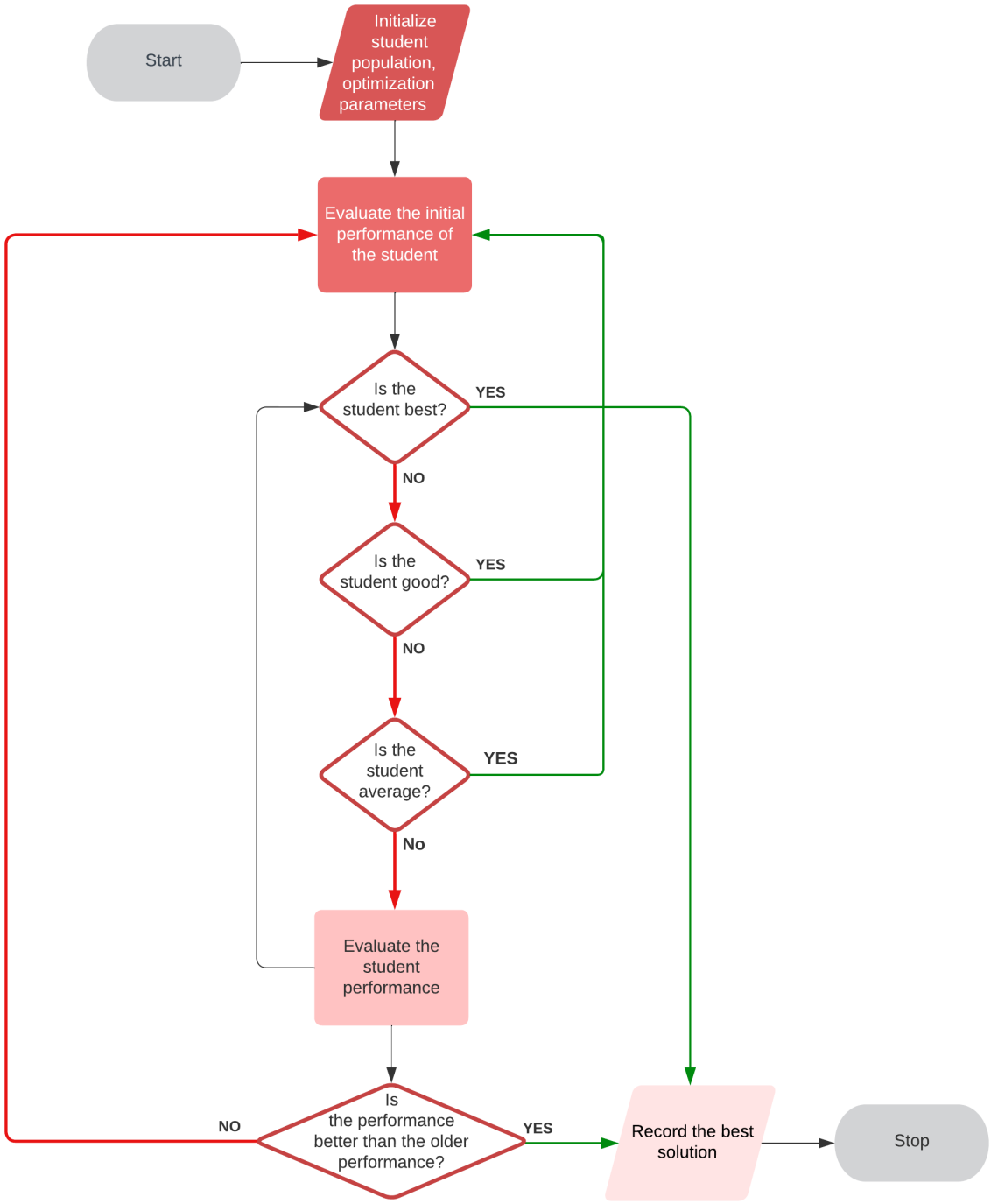

FIGURE 11. Flowchart of the SPBOA.

controller gains for both models. Time-domain analysis is performed on the simulation models under three different types of load perturbations (refer Fig. 8). The adopted parameters of the proposed SPBOA and QOWOA are presented in Table A.3 – A.4 of the Appendix Section. Here, performance studies were executed for two cases, as mentioned below. *Case I:* For this case, the performance analysis of the studied IHPS-I model is carried out considering three load perturbations shown in Fig.8. The following six scenarios are considered in this case:

Scenario I: Variation in load: (a) a 10% increase in step load perturbation (SLP) and (b) an increase in random SLP (RSLP).

Scenario II: Load Variation: (a) a 10% reduction in SLP and (b) a reduction in RSPL.

Scenario III: Random change in load perturbation (RLP).

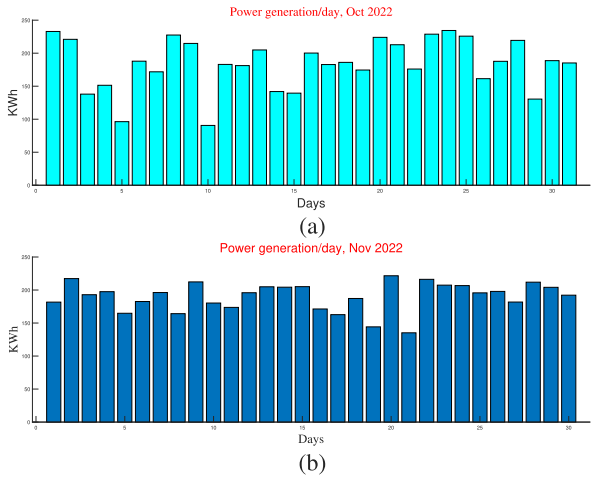

FIGURE 12. Monthly power generation report of 40 KWp solar power plant.

Scenario IV: Unpredictable changes in wind perturbation.
Scenario V: Load changes at random and wind perturbation.
Scenario VI: Unpredictable changes in wind particulate and SPV output.

Case II: For this case, the performance analysis is of the IHPS-II model. In this case, the following three scenarios are considered.

Scenario VII: 10 % increase in step load disturbance.

Scenario VIII: Increased load disturbance due to random step perturbation.

Scenario IX: Random perturbation increases load disturbance.

A. PERFORMANCE ANALYSIS OF CASE I

In this section, the focus has been given to analyzing the dynamic performance of the IHPS-I with the solar PV power plant, taking into account various load and wind perturbations. Fig. 9 presents the *P-V* and *I-V* characteristics of a solar PV module under different operating conditions for both the IHPS-I and IHPS-II systems. Specifically, Figs. 9(a) and (b) depict the *P vs V* and the *I vs V* characteristics of a solar PV module at a constant temperature of 25^o C and various levels of solar irradiation (considered as 1000, 800, 600 W/m^2). while Figs. 9(c) and (d) illustrate the *P vs V* and *I vs V* characteristics of a solar PV module under 1000 W/m^2 irradiation and at various temperatures (such as 25°, 35°, 45° C).

The DC-DC boost converter under STC is composed of a bus capacitor of 1670 uF, a filter capacitor of 2 mF, a resistance of 23.14 ohm, and an N-channel MOSFET as the switching component operating at a frequency of 20 kHz. Depending on the prevailing weather conditions, an IC algorithm-based MPPT generates the duty cycle, which is then passed through the pulse width modulation to obtain the gate pulse required for the MOSFET of the boost converter.

The 40 KWp solar PV system's monthly power generation data for the months of October and November 2022 are depicted in Fig.12. In October and November, the total power produced was 5516.2 KWh and 5709.8 KWh, respectively. For the above-considered months, the average daily power generation is approximately 177 KWh and 190 kWh, respectively.

To ensure good dynamic stability of the IHPS-I model, optimized PID controllers have been employed. The gains of the PID controllers are optimized using the proposed SPBOA and QOWOA methods to maximize the output from the system. ITAE of frequency deviation has been considered as the objective function, and the controller gains are in the range of 0.001 to 2. The outcomes of concern are marked in boldface in their respective scenarios. The IHPS-I system shown in Fig. 1 was subjected to two load patterns, analyzed using *Scenario I*. The first was a sudden increase in SLP of 10% (0.1 p.u.), while the second was an RSLP increase in load, illustrated in Figs. 8 (a) and (b). The SPBOA and QOWOA were employed to optimize the PID controller gains for both load patterns, running for 100 iterations. Figs. 13 (a) to (c) depicts the power generated from DEG, PV, and WTG, while Figs. 13 (d) to (f) illustrate the dynamic responses of frequency deviation profiles and FOD mobility. The compared frequency responses for 0.1 p.u. step load demands for the proposed SPBOA-based model and the QOWOA-based model are presented in Fig. 13 (d). From the figure, the peak, rise time, settling time, peak time, and steady-state error are 0.2391, 0.0134, 19.6029, 1.000, and 0.00005, respectively for the QOWOA-based model. The QOWOA-based model's performance indices are presented in Table 3. In Fig. 13 (f), the FOD values for the 0.1 p.u. a step increase in load demand have been compared, and it has been seen that the proposed SPBOA-based model gives a better value (**6.9140**) than the value (7.2626) of the QOWOA-based model. Tables 1 and 2 list the optimal values of the PID controller gains and performance indices, along with the objective function.

The simulation results of *Scenario II* are illustrated in Fig. 14, showing the frequency deviation profiles of the IHPS-I model obtained with (a) a sudden SLP decrease in load demand exposed to a step decrease in load demand and (b) an RSLP decrease in load demand. Tables 1 - 3 present the optimized gains of the PID controller, performance indices, and dynamic performance analysis. While comparing the FOD mobility of this scenario with the others, it may be observed that the FOD value is **13.3068** and **14.2452** for the proposed SPBOA and QOWOA-based models.

In *Scenarios III-VI*, random load perturbation (Fig. 8c), random wind perturbation, and random load and wind perturbation were applied to the IHPS-I model. Figs. 15a - c show the SPBOA and QOWOA-based comparative frequency deviation profiles, as well as the FOD convergence profile, for *Scenarios III*. Figs. 16a - c, represent the frequency deviation profile, SPBOA and QOWOA-based comparative convergence profile of FOD for *Scenario IV*. The relative time-domain analysis of the frequency plot is carried out and the convergence plot of the proposed SPBOA and QOWOA for *Scenario V* is shown in Figs. 17a - b,

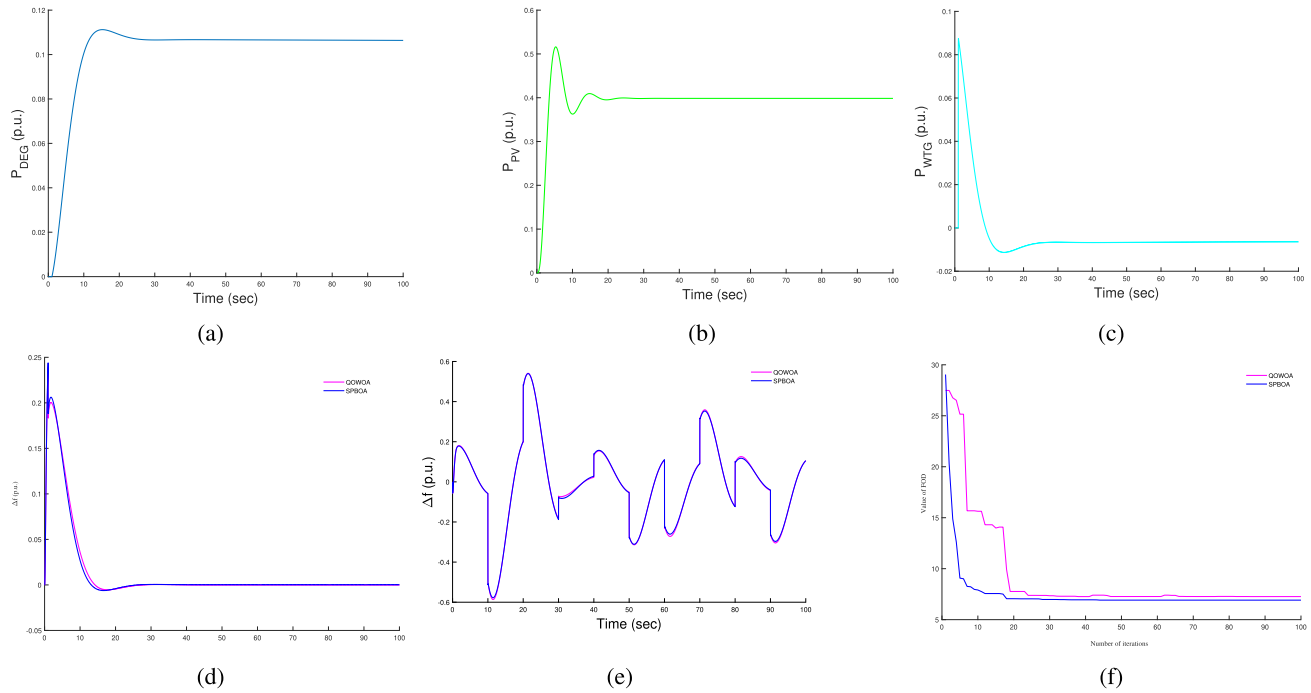

FIGURE 13. Dynamic response profile of Δf (p.u) pertaining to Scenario I (a) $P_{DEG}(p.u.)$, $(b)P_{PV}$ (p.u.), (c) P_{WTG} (p.u.), (d)10% increase in SLP, (e) increase in RSLP and (f) QOWOA and SPBOA based FOD mobility.

TABLE 1. Optimized parameters for the studied models for IHPS-I configuration pertaining to Case I.

Controllers	Gain parameters	Scenario I (a)		Scenario I(b)		Scenario II(a)		Scenario II(b)		Scenario III		Scenario IV		Scenario V		Scenario VI	
		QOWOA	SPBOA	QOWOA	SPBOA	QOWOA	SPBOA	QOWOA	SPBOA	QOWOA	SPBOA	QOWOA	SPBOA	QOWOA	SPBOA	QOWOA	SPBOA
Controller I	K_{PD}	2.0000	2.0000	2.0000	2.0000	2.0000	2.0000	2.0000	2.0000	2.0000	2.0000	2.0000	2.0000	2.0000	2.0000	2.0000	2.0000
	K_{ID}	0.5627	0.5940	0.4989	1.5254	0.5829	0.5941	1.5910	1.5757	0.6081	0.5967	0.5679	0.6014	0.5853	0.6019	0.6120	0.5910
	K_{DD}	0.0460	0.0109	2.0000	2.0000	0.8873	0.0104	2.0000	2.0000	1.0220	0.0100	0.4498	0.0100	0.2937	0.1750	0.6299	0.6240
Controller II	K_{PW}	0.0010	0.0100	0.0010	0.0100	0.0028	0.0100	0.0010	0.0100	1.1126	0.0100	2.0000	0.0100	0.2368	0.0100	0.2725	0.1252
	K_{IW}	0.0010	0.0100	0.0010	0.0100	0.0023	0.0100	0.0010	0.0100	0.4819	0.0100	0.5734	0.0100	0.0013	0.0100	0.6856	0.4250
	K_{DW}	0.0010	2.0000	1.0974	0.0100	0.0028	2.0000	0.0010	0.0100	0.5131	2.0000	0.6828	2.0000	0.6661	1.9987	0.6227	2.0000

TABLE 2. Objective function values and performance indices for Case I.

Indices	Scenario I (a)		Scenario I (b)		Scenario II (a)		Scenario II (b)		Scenario III		Scenario IV		Scenario V		Scenario VI	
	QOWOA	SPBOA	QOWOA	SPBOA	QOWOA	SPBOA	QOWOA	SPBOA	QOWOA	SPBOA	QOWOA	SPBOA	QOWOA	SPBOA	QOWOA	SPBOA
ISE	0.1981	**0.1957**	4.4144	**4.3508**	0.5736	**0.5996**	3.5055	**3.4916**	0.2192	**0.1924**	0.2472	**0.1839**	0.5858	**0.1810**	0.2451	**0.2243**
ITSE	0.6739	**0.6288**	164.242	**160.5983**	2.3139	**2.2553**	143.7657	**143.240**	0.9337	**0.6946**	1.0408	**0.6221**	2.2243	**0.6884**	0.6973	**0.5931**
IAE	1.3880	**1.3411**	15.3438	**15.2914**	2.4948	**2.4413**	14.3809	**14.3603**	1.6284	**1.3688**	1.7120	**1.3388**	2.4794	**1.3604**	1.5756	**1.4829**
ITAE (J)	7.2626	**6.9140**	684.560	**678.858**	14.2452	**13.3068**	652.0770	**651.632**	11.2998	**7.4891**	10.9162	**7.6730**	13.3752	**8.0461**	11.3408	**9.7392**

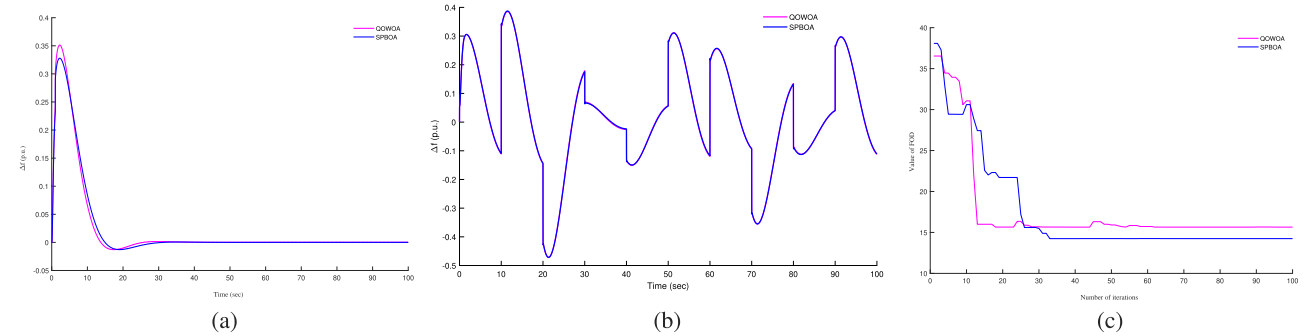

FIGURE 14. Dynamic response profile of (p.u) pertaining to Scenario II (a) 10% decrease in SLP, (b) decrease in RSLP and (c) QOWOA and SPBOA based FOD mobility.

respectively. In *Scenario VI*, comparative frequency response and FOD mobility based on QOWOA and SPBOA are pertaining in Figs. 18a - b. Tables 1 and 2 provide the controller gains of the studied models and the performance indices like ISE, ITSE, IAE, and the objective function ITAE (J).

TABLE 3. QOWOA-based performance analysis of IHPS-I configuration pertaining to Case I.

Studied scenarios	M_P (%)	t_r (sec)	t_s(sec)	t_p (sec)	e_{ss}
Scenario-I (a)	0.2391	0.0134	19.6029	1.0000	0.00005
Scenario-I (b)	0.5867	0.2765	99.3579	11.5068	0.10490
Scenario-II (a)	0.3279	0.0141	24.2836	2.2447	0.00005
Scenario-II (b)	0.4720	2.1299	99.4955	21.3041	-0.1125
Scenario-III	0.1946	0.0663	24.5714	2.3095	0.00001
Scenario-IV	0.2208	0.0017	23.6644	1.0000	0.00010
Scenario-V	0.1831	0.0005	24.5076	2.4469	0.00023
Scenario-VI	0.2179	0.0015	28.4173	0.2179	0.00010

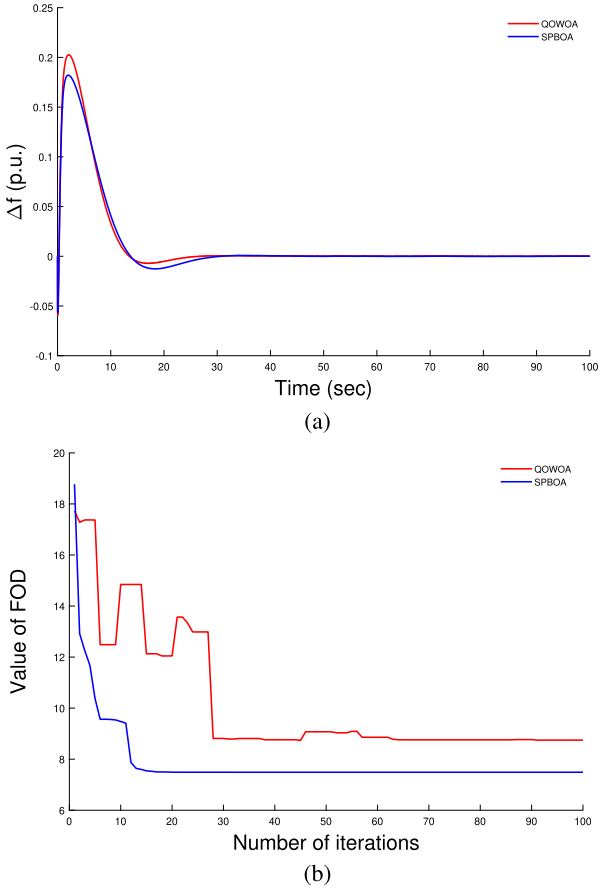

FIGURE 15. Characteristic pertaining to Scenario III of (a) Δf (p.u) for RLP increase and (b) QOWOA and SPBOA based FOD mobility.

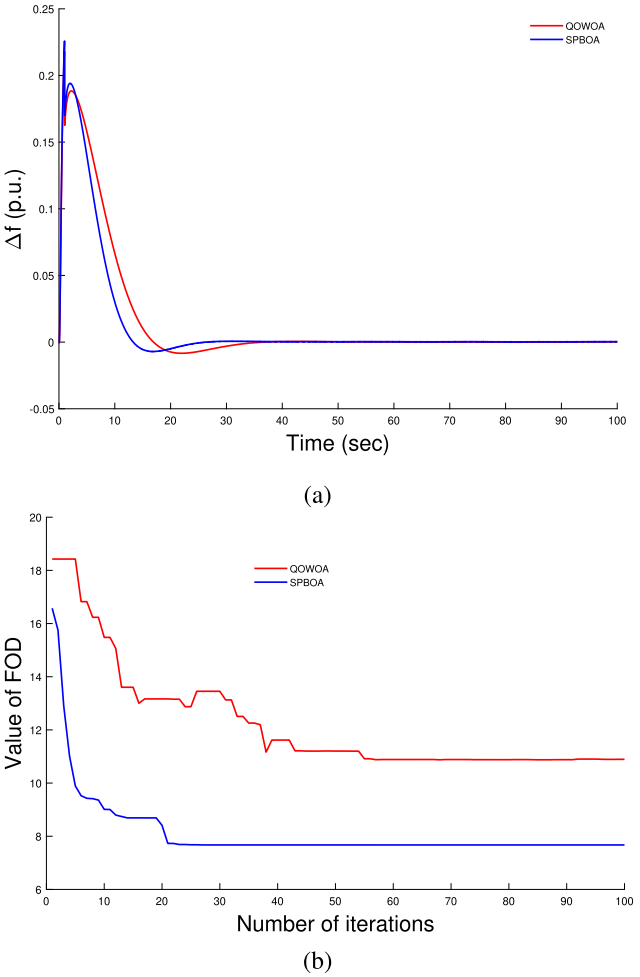

FIGURE 16. Characteristic pertaining to Scenario IV of (a) Δf (p.u) for random wind perturbation and (b) QOWOA and SPBOA based FOD mobility.

It is evident from *Scenarios III-VI* that the frequency oscillations were attenuated after **24.5717** sec, **23.6644** sec, **24.5076** sec and **28.4173** sec, respectively, and then the system has reached its steady state conditions. It is also observed that the FOD values of *Scenarios III-VI* for SPBO and QOWOA based models were **7.4891**, **7.6730**, **8.0461**, **9.7392** and **11.2998**, **10.9162**, **13.3752**, **11.3408** individually.

Overall, the results showed that the SPBOA optimized PID controller outperformed in terms of FOD minimization, as seen from Figs. 13- 18 and Table 2.

B. PERFORMANCE ANALYSIS OF CASE II

The focus of this study is on the IHPS-II model, which includes an STPP, a WTG, and solar PV. The study analyzes the time-domain performance of the IHPS-II model under different load conditions *Scenarios VII-IX*.

Scenario VII involves running the IHPS-II model for 100 seconds with a 10% SLP, as shown in Fig. 8a). *Scenario VIII*, on the other hand, involves applying RSLP to IHPS-II for 100 seconds, as illustrated in Fig. 8b. In this scenario, RSLP input increases initially up to 20 sec, then decreases to 40 sec, then increases to 70 sec, and again decreases to 90 sec, then increases to 100 sec. Every increment and decrement occurs every 10 seconds, with a maximum load change of 1.0 p.u. and a minimum load change of 0.1 p.u.

For the final scenario, *Scenario IX*, the model is subjected to RLP for 100 seconds as shown in Fig. 8c. In all scenarios, each power-generating unit in the IHPS-II model is equipped with a PID controller, with its parameters tuned by SPBOA and QOWOA.

The comparative frequency deviation profiles of *Scenarios VII*, *VIII*, and *IX* are shown in Figs. 19- 21, with Fig. 19a, 20a and 21a, representing *Scenarios VII, VIII*, and *IX*,

TABLE 4. Optimized tuned parameters for the studied models for IHPS-I configuration pertaining to Case II.

Controllers	Gain parameters	Scenario VII		Scenario VIII		Scenario IX	
		QOWOA	SPBOA	QOWOA	SPBOA	QOWOA	SPBOA
Controller I	K_{PT}	2.0000	*2.0000*	2.0000	2.0000	2.0000	2.0000
	K_{IT}	2.0000	*2.0000*	2.0000	2.0000	2.0000	2.0000
	K_{DT}	0.0013	*0.0100*	0.0010	0.0100	0.0010	0.0100
Controller II	K_{PW}	0.0012	*0.0100*	0.0010	0.0100	0.0024	0.0100
	K_{IW}	1.5109	*1.6469*	2.0000	0.0100	2.0000	1.6506
	K_{DW}	0.0233	*2.0000*	2.0000	0.0100	2.0000	2.0000

TABLE 5. Objective function values and performance indices for Case II.

Indices	Scenario VII		Scenario VIII		Scenario IX	
	QOWOA	SPBOA	QOWOA	SPBOA	QOWOA	SPBOA
ISE	0.0800	0.0842	0.0999	0.0914	0.0848	0.0840
ITSE	0.1265	0.1319	0.0747	0.6672	0.1359	0.1337
IAE	0.5607	0.5628	1.2136	1.1427	0.5745	0.5623
ITAE (J)	1.5716	1.4709	33.1658	30.3461	1.6344	1.4921

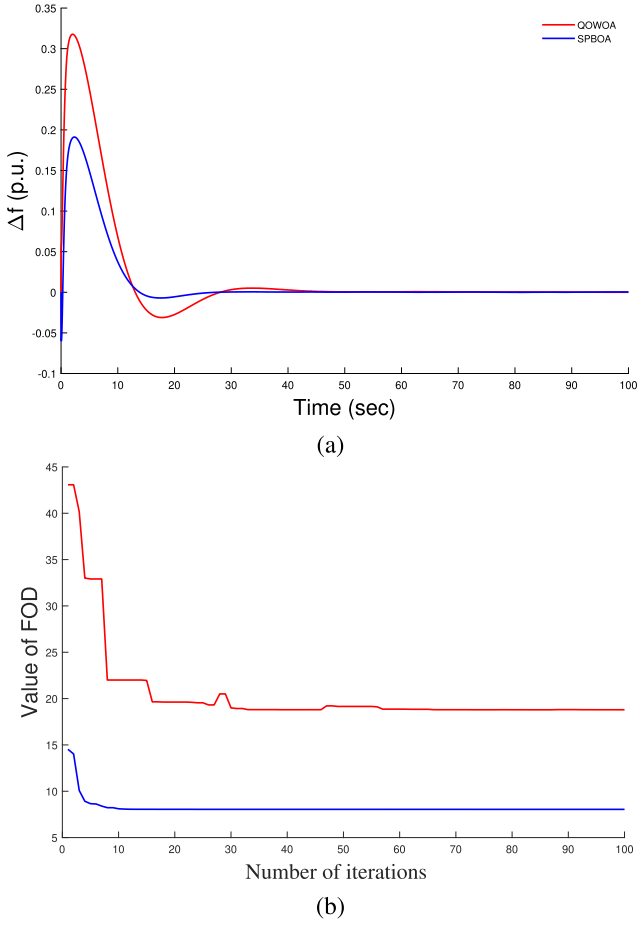

FIGURE 17. Characteristic pertaining to Scenario V of (a) Δf (p.u) for random load and wind perturbation and (b) QOWOA and SPBOA-based FOD mobility.

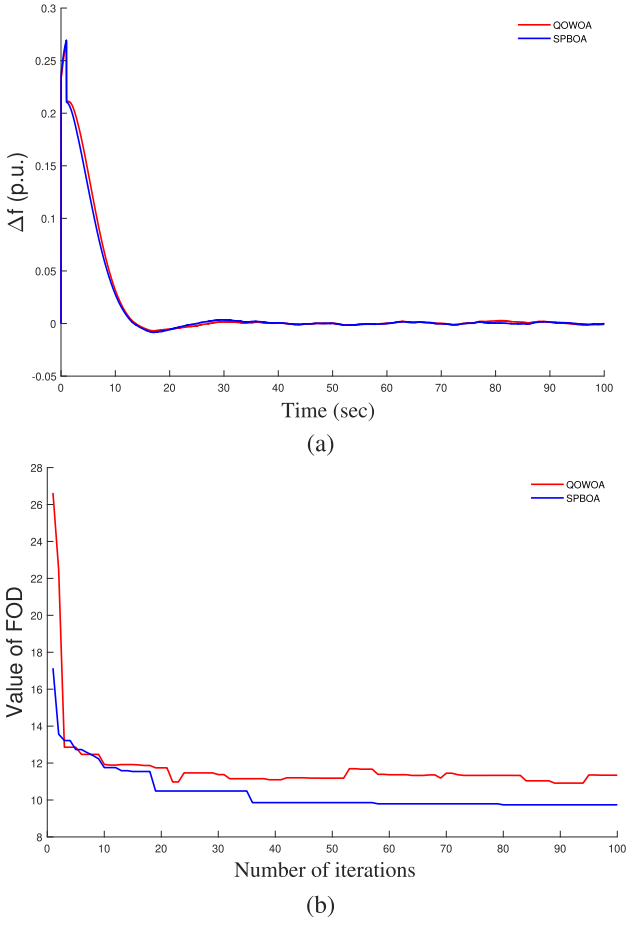

FIGURE 18. Characteristic pertaining to Scenario VI of (a) Δf (p.u) for Random change in wind perturbation and solar PV output and (b) QOWOA and SPBOA-based FOD mobility.

respectively. The comparative convergence motilities of the FOD values obtained by the proposed SPBOA and QOWOA are illustrated in Figs. 19b, 20b and 21b, in order, for the aforementioned scenarios.

Table 4 represents the QOWOA-based optimized PID controller gains for *Scenarios VII-IX*. It is observed that the SPBOA-based FOD values for Scenarios VII-IX are lower than the QOWOA-based FOD values, as shown in Table 5.

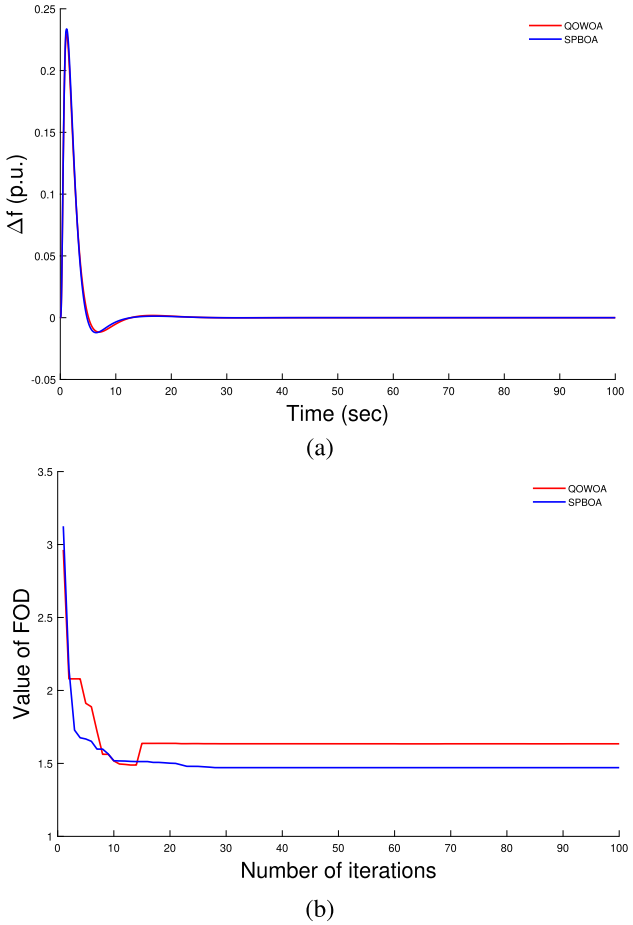

FIGURE 19. Characteristic pertaining to Scenario VII of (a) Δf (p.u) for 10 % increase in SLP and (b) QOWOA and SPBOA based FOD mobility.

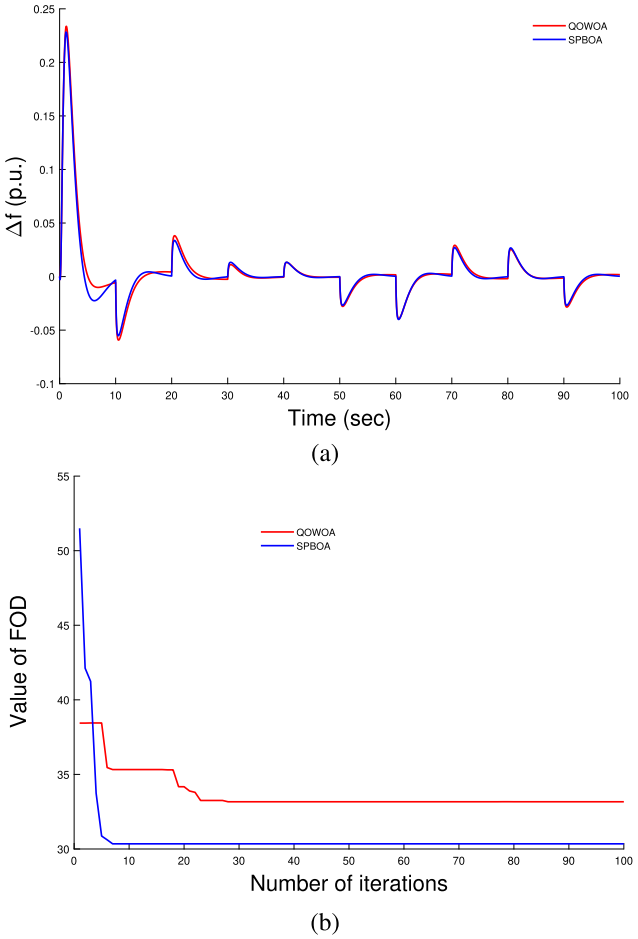

FIGURE 20. Characteristic pertaining to Scenario VIII of (a) Δf (p.u) for the increase in RSLP and (b) QOWOA and SPBOA-based FOD mobility.

TABLE 6. Optimized tuned parameters for the studied models for IHPS-I configuration pertaining to Case II.

Studied scenarios	M_P (%)	t_r (sec)	t_s(sec)	t_p (sec)	e_{ss}
Scenario VII	0.2298	0.0037	10.2081	1.0761	-0.0010
Scenario VIII	0.2337	0.0133	93.2934	1.1987	0.0018
Scenario IX	0.2337	0.0099	10.5990	1.2110	-0.0027

TABLE 7. Nominal system parameters of the studied IHPS-I and IHPS-II models.

Model	Parameters			
Wind unit	K_{P1} =1.25 K_{IG} =0.9969 T_{P3} =1.00 sec	K_{P2} =1.00 K_{PC} =0.080	K_{P3} =1.40 T_{P1} =0.80 sec	K_{TP}=0.0033 T_{P2} =0.041 sec
Diesel unit	K_D =0.3333 T_D3 =0.025 sec	R_D =3.0 Hz/pu T_D4=3.00 sec	T_D1 =1.00 sec	T_D2=2.00 sec
Thermal units	T_g=0.8 sce	T_t=0.3 sec	R_D =2.4 Hz/pu	
Power system unit	K_P =120	T_P =14.4 sec		

The performance analysis of *Scenarios VII-IX* is presented in Table 6, with the peak overshoot of *Scenario VII* being 0.2298 and 0.2337 for *Scenarios VIII and IX*.

Overall, this study provides valuable insights into the time-domain performance of the IHPS-II model under different load conditions and highlights the effectiveness of the proposed SPBOA and QOWOA techniques for tuning the PID controller parameters.

TABLE 8. Nominal system parameters of the studied Solar PV model.

Parameters	Description	Values
P_{max}	Nominal maximum power	350 W
V_{mp}	Optimum operating voltage	39.2 V
I_{mp}	Optimum operating current	8.94 A
V_{oc}	Open circuit voltage	46.6 V
I_{sc}	Short circuit current	9.51 A

TABLE 9. Parameters of the SPBOA and QOWOA.

Method	Parameters	Values
SPBOA	Number of variable	06
	No of the students	10
	Dimension of the problem	5
	Number of iteration	100
QOWOA	Number of search agent	10
	Jumping rate	0.8
	Dimension of the problem	5
	Number of iteration	100

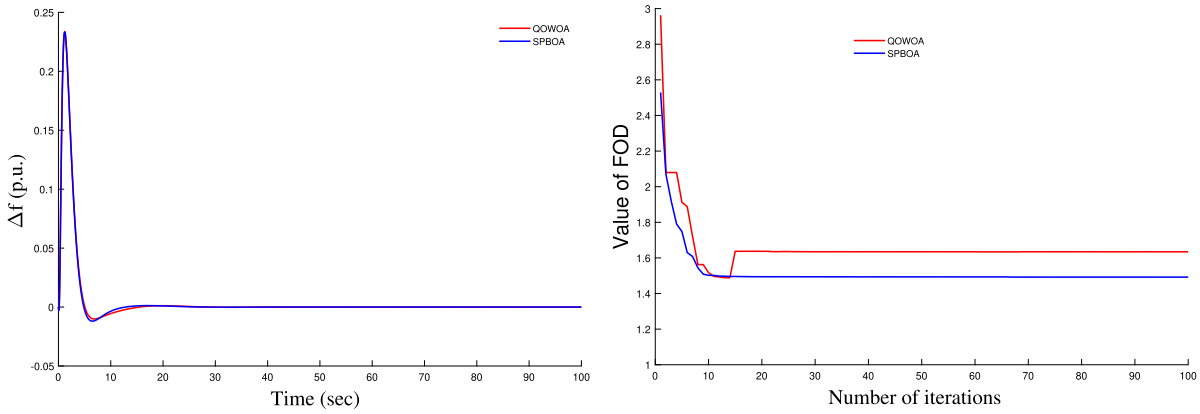

FIGURE 21. Characteristic pertaining to Scenario IX of (a) Δf (p.u) for the increase in RLP and (b) QOWOA and SPBOA-based FOD mobility.

VI. CONCLUSION AND SCOPES OF FUTURE WORK

This research investigates the load frequency control of two renewable energy-based power systems, the IHPS-I and IHPS-II models. The study aims to explore the impact of different uncertainties on the load demand, solar and wind inputs, and propose an optimal solution to enhance the control of these power systems for rural electrification. The SPBOA and QOWOA optimization algorithms are used to achieve the global optimal solution of the power system model. Classical PID controllers are used to control the DEG's governor and the WTG's pitch angle in the IHPS-I model and the STPP's governor in the IHPS-II model. The simulation models are carried out for time-domain analysis under various load scenarios. The study reveals that the SPBOA-based model reduced the value of ITAE by nearly 5%, and the peak and settling time of the frequency response have been minimized by 5%-7% compared to the QOWOA-based model. The results provide valuable insights into the optimal control of renewable energy-based power systems for rural electrification.

Future work could include exploring the impact of other uncertainties, such as variations in solar irradiance and wind speed, on load frequency control. Additionally, integrating energy storage systems, conducting a techno-economic analysis, and investigating larger-scale power systems could be useful. Continued research in renewable energy-based power systems can significantly improve access to reliable and sustainable energy in rural areas.

APPENDIX

The nominal system parameters of the studied IHPS-I and II models are furnished in Table 7. Table 8 includes the nominal system parameters of the studied solar PV model. The parameters of the proposed QOWOA and SPBOA are included in Table 9.

ACKNOWLEDGMENT

The authors thank Dr. Ben Othman Soufiene.

REFERENCES

[1] R. Tang, Z. Wu, and Y. Fang, "Configuration of marine photovoltaic system and its MPPT using model predictive control," *Sol. Energy*, vol. 158, pp. 995–1005, Dec. 2017.

[2] A. S. Eisa, "Nonlinear modeling, analysis and simulation of wind turbine control system with and without pitch control as in industry," in *Advanced Control and Optimization Paradigms for Wind Energy Systems*. 2019, pp. 1–40.

[3] S. A. Mousavi, M. Mehrpooya, M. A. V. Rad, and M. H. Jahangir, "A new decision-making process by integration of exergy analysis and techno-economic optimization tool for the evaluation of hybrid renewable systems," *Sustain. Energy Technol. Assessments*, vol. 45, Jun. 2021, Art. no. 101196.

[4] S. A. Mousavi, R. A. Zarchi, F. R. Astaraei, R. Ghasempour, and F. M. Khaninezhad, "Decision-making between renewable energy configurations and grid extension to simultaneously supply electrical power and fresh water in remote villages for five different climate zones," *J. Cleaner Prod.*, vol. 279, Jan. 2021, Art. no. 123617.

[5] Y. Mi, C. Ma, Y. Fu, C. Wang, P. Wang, and P. C. Loh, "The SVC additional adaptive voltage controller of isolated wind-diesel power system based on double sliding-mode optimal strategy," *IEEE Trans. Sustain. Energy*, vol. 9, no. 1, pp. 24–34, Jan. 2018.

[6] J. Li, R. Xiong, Q. Yang, F. Liang, M. Zhang, and W. Yuan, "Design/test of a hybrid energy storage system for primary frequency control using a dynamic droop method in an isolated microgrid power system," *Appl. Energy*, vol. 201, pp. 257–269, Sep. 2017.

[7] B. Raouf, A. Akbarimajd, A. Dejamkhooy, and S. SeyedShenava, "Robust distributed control of reactive power in a hybrid wind-diesel power system with STATCOM," *Int. Trans. Elect. Energy Syst.*, vol. 29, no. 4, 2019, Art. no. e2780, doi: 10.1002/etep.2780.

[8] M. A. M. Ramli, H. R. E. H. Bouchekara, and A. S. Alghamdi, "Optimal sizing of PV/wind/diesel hybrid microgrid system using multi-objective self-adaptive differential evolution algorithm," *Renew. Energy*, vol. 121, pp. 400–411, Jun. 2018.

[9] F. Alvarez-Mendoza, C. Angeles-Camacho, P. Bacher, and H. Madsen, "Semi-dispatchable generation with wind-photovoltaic-fuel cell hybrid system to mitigate frequency disturbance," *Electr. Power Syst. Res.*, vol. 165, pp. 60–67, Dec. 2018.

[10] J. Jurasz, J. Mikulik, M. Krzywda, B. Ciapała, and M. Janowski, "Integrating a wind- and solar-powered hybrid to the power system by coupling it with a hydroelectric power station with pumping installation," *Energy*, vol. 144, pp. 549–563, Feb. 2018.

[11] C. Ghenai, A. Merabet, T. Salameh, and E. C. Pigem, "Grid-tied and stand-alone hybrid solar power system for desalination plant," *Desalination*, vol. 435, pp. 172–180, Jun. 2018.

[12] T. Sarkar, A. Bhattacharjee, H. Samanta, K. Bhattacharya, and H. Saha, "Optimal design and implementation of solar PV-wind-biogas-VRFB storage integrated smart hybrid microgrid for ensuring zero loss of power supply probability," *Energy Convers. Manage.*, vol. 191, pp. 102–118, Jul. 2019.

[13] H. Nizamuddin, I. Nasiruddin, T. S. Bhatti, and Y. Arya, "Optimal automatic generation control with hydro, thermal, gas, and wind power plants in 2-area interconnected power system," *Electr. Power Compon. Syst.*, vol. 48, nos. 6–7, pp. 558–571, 2020, doi: 10.1080/15325008.2020.1793829.

[14] P. K. Pathak, A. K. Yadav, S. Padmanaban, and I. Kamwa, "Fractional cascade LFC for distributed energy sources via advanced optimization technique under high renewable shares," *IEEE Access*, vol. 10, pp. 92828–92842, 2022, doi: 10.1109/ACCESS.2022.3202907.

[15] M. Ramesh, A. K. Yadav, and P. K. Pathak, "Artificial gorilla troops optimizer for frequency regulation of wind contributed microgrid system," *J. Comput. Nonlinear Dyn.*, vol. 18, no. 1, Jan. 2023, Art. no. 011005, doi: 10.1115/1.4056135.

[16] H. Fathabadi, "Novel standalone hybrid solar/wind/fuel cell power generation system for remote areas," *Sol. Energy*, vol. 146, pp. 30–43, Apr. 2017.

[17] P. K. Pathak and A. K. Yadav, "Design of optimal cascade control approach for LFM of interconnected power system," *ISA Trans.*, vol. 137, pp. 506–518, Jun. 2023, doi: 10.1016/j.isatra.2023.01.029.

[18] S. Ranjan, D. Chandra Das, S. Behera, and N. Sinha, "Parabolic trough solar–thermal–wind–diesel isolated hybrid power system: Active power/frequency control analysis," *IET Renew. Power Gener.*, vol. 12, no. 16, pp. 1893–1903, Dec. 2018.

[19] A. Rahman, L. C. Saikia, and N. Sinha, "Automatic generation control of an interconnected two-area hybrid thermal system considering dish-stirling solar thermal and wind turbine system," *Renew. Energy*, vol. 105, pp. 41–54, May 2017.

[20] D. K. Mishra, T. K. Panigrahi, A. Mohanty, and P. K. Ray, "Impact of wind/solar integration on frequency control in two-area power system," in *Proc. 19th Int. Carpathian Control Conf. (ICCC)*, May 2018, pp. 580–584, doi: 10.1109/CarpathianCC.2018.8399697.

[21] S. M. Abd-Elazim and E. S. Ali, "Firefly algorithm-based load frequency controller design of a two area system composing of PV grid and thermal generator," *Electr. Eng.*, vol. 100, no. 2, pp. 1253–1262, Jun. 2018.

[22] H. M. Hasanien and A. A. El-Fergany, "Salp swarm algorithm-based optimal load frequency control of hybrid renewable power systems with communication delay and excitation cross-coupling effect," *Electr. Power Syst. Res.*, vol. 176, Nov. 2019, Art. no. 105938.

[23] E. Çelik, N. Öztürk, and Y. Arya, "Advancement of the search process of salp swarm algorithm for global optimization problems," *Expert Syst. Appl.*, vol. 182, Nov. 2021, Art. no. 115292, doi: 10.1016/j.eswa.2021.115292.

[24] H. H. Ali, A. M. Kassem, M. Al-Dhaifallah, and A. Fathy, "Multi-verse optimizer for model predictive load frequency control of hybrid multi-interconnected plants comprising renewable energy," *IEEE Access*, vol. 8, pp. 114623–114642, 2020.

[25] J. Mudi, C. K. Shiva, B. Vedik, and V. Mukherjee, "Frequency stabilization of solar thermal-photovoltaic hybrid renewable power generation using energy storage devices," *Iranian J. Sci. Technol., Trans. Electr. Eng.*, vol. 45, no. 2, pp. 597–617, Jun. 2021.

[26] R. Rajan, F. M. Fernandez, and Y. Yang, "Primary frequency control techniques for large-scale PV-integrated power systems: A review," *Renew. Sustain. Energy Rev.*, vol. 144, Jul. 2021, Art. no. 110998.

[27] D. Yousri, T. S. Babu, and A. Fathy, "Recent methodology based Harris hawks optimizer for designing load frequency control incorporated in multi-interconnected renewable energy plants," *Sustain. Energy, Grids Netw.*, vol. 22, Jun. 2020, Art. no. 100352.

[28] K. K. Sahoo, R. Ghosh, S. Mallik, A. Roy, P. K. Singh, and Z. Zhao, "Wrapper-based deep feature optimization for activity recognition in the wearable sensor networks of healthcare systems," *Sci. Rep.*, vol. 13, no. 1, p. 965, Jan. 2023, doi: 10.1038/s41598-022-27192-w.

[29] M. A. Nasab, M. Zand, S. Padmanaban, M. S. Bhaskar, and J. M. Guerrero, "An efficient, robust optimization model for the unit commitment considering renewable uncertainty and pumped-storage hydropower," *Comput. Electr. Eng.*, vol. 100, May 2022, Art. no. 107846, doi: 10.1016/j.compeleceng.2022.107846.

[30] S. Ganguly, T. Mahto, and V. Mukherjee, "Integrated frequency and power control of an isolated hybrid power system considering scaling factor based fuzzy classical controller," *Swarm Evol. Comput.*, vol. 32, pp. 184–201, Feb. 2017.

[31] M. Khalili, M. Ali Dashtaki, M. A. Nasab, H. Reza Hanif, S. Padmanaban, and B. Khan, "Optimal instantaneous prediction of voltage instability due to transient faults in power networks taking into account the dynamic effect of generators," *Cogent Eng.*, vol. 9, no. 1, Dec. 2022, Art. no. 2072568, doi: 10.1080/23311916.2022.2072568.

[32] M. A. Nasab, M. Zand, A. Hatami, F. Nikoukar, S. Padmanaban, and A. H. Kimiai, "A hybrid scheme for fault locating for transmission lines with TCSC," in *Proc. Int. Conf. Protection Autom. Power Syst. (IPAPS)*, Zahedan, Iran, Jan. 2022, pp. 1–10, doi: 10.1109/IPAPS55380.2022.9763217.

[33] M. Zand, M. A. Nasab, M. Khoobani, A. Jahangiri, S. H. Hosseinian, and A. H. Kimiai, "Robust speed control for induction motor drives using STSM control," in *Proc. 12th Power Electron., Drive Syst., Technol. Conf. (PEDSTC)*, Tabriz, Iran, Feb. 2021, pp. 1–6, doi: 10.1109/PEDSTC52094.2021.9405912.

[34] B. Das, V. Mukherjee, and D. Das, "Student psychology based optimization algorithm: A new population based optimization algorithm for solving optimization problems," *Adv. Eng. Softw.*, vol. 146, Aug. 2020, Art. no. 102804.

[35] J. Mudi, C. K. Shiva, and V. Mukherjee, "An optimal control of integrated hybrid power system with FACTS devices using student psychology-based optimization algorithm," *Adv. Theory Simul.*, vol. 4, no. 9, Sep. 2021, Art. no. 2100147.

[36] R. Roy, V. Mukherjee, and R. P. Singh, "Model order reduction of proton exchange membrane fuel cell system using student psychology based optimization algorithm," *Int. J. Hydrogen Energy*, vol. 46, no. 75, pp. 37367–37378, 2021.

[37] K. Balu and V. Mukherjee, "Optimal siting and sizing of distributed generation in radial distribution system using a novel student psychology-based optimization algorithm," *Neural Comput. Appl.*, vol. 33, pp. 15639–15667, Jun. 2021.

[38] S. Mirjalili and A. Lewis, "The whale optimization algorithm," *Adv. Eng. Softw.*, vol. 95, pp. 51–67, May 2016.

[39] H. R. Tizhoosh, "Opposition-based learning: A new scheme for machine intelligence," in *Proc. Int. Conf. Comput. Intell. Modeling, Control Autom. Int. Conf. Intell. Agents, Web Technol. Internet Commerce (CIMCA-IAWTIC)*, 2005, pp. 695–701.

[40] T. Si, D. Bhattacharya, S. Nayak, P. B. C. Miranda, U. Nandi, S. Mallik, U. Maulik, and H. Qin, "PCOBL: A novel opposition-based learning strategy to improve metaheuristics exploration and exploitation for solving global optimization problems," *IEEE Access*, vol. 11, pp. 46413–46440, 2023, doi: 10.1109/ACCESS.2023.3273298.

[41] S. Rahnamayan, H. R. Tizhoosh, and M. M. A. Salama, "Quasi-oppositional differential evolution," in *Proc. IEEE Congr. Evol. Comput.*, Sep. 2007, pp. 2229–2236.

[42] S. Ganguly and V. Mukherjee, "Frequency stabilization of isolated hybrid power system by a novel quasi-oppositional whale optimization algorithm," *Iranian J. Sci. Technol., Trans. Electr. Eng.*, vol. 44, no. 4, pp. 1467–1486, Dec. 2020.

[43] S. Ganguly, C. K. Shiva, and V. Mukherjee, "Frequency stabilization of isolated and grid connected hybrid power system models," *J. Energy Storage*, vol. 19, pp. 145–159, Oct. 2018.

[44] Z. Roumila, D. Rekioua, and T. Rekioua, "Energy management based fuzzy logic controller of hybrid system wind/photovoltaic/diesel with storage battery," *Int. J. Hydrogen Energy*, vol. 42, no. 30, pp. 19525–19535, Jul. 2017.

[45] V. R. Kota and M. N. Bhukya, "A novel linear tangents based P&O scheme for MPPT of a PV system," *Renew. Sustain. Energy Rev.*, vol. 71, pp. 257–267, May 2017.

[46] A. M. Farayola, A. N. Hasan, and A. Ali, "Implementation of modified incremental conductance and fuzzy logic MPPT techniques using MCUK converter under various environmental conditions," *Appl. Sol. Energy*, vol. 53, no. 2, pp. 173–184, Apr. 2017.

[47] U. Yilmaz, A. Kircay, and S. Borekci, "PV system fuzzy logic MPPT method and PI control as a charge controller," *Renew. Sustain. Energy Rev.*, vol. 81, pp. 994–1001, Jan. 2018.

[48] C. Dhakhinamoorthy, S. K. Mani, S. K. Mathivanan, S. Mohan, P. Jayagopal, S. Mallik, and H. Qin, "Hybrid whale and gray wolf deep learning optimization algorithm for prediction of Alzheimer's disease," *Mathematics*, vol. 11, no. 5, p. 1136, Feb. 2023, doi: 10.3390/math11051136.

[49] M. Abdel-Basset, G. Manogaran, D. El-Shahat, and S. Mirjalili, "RETRACTED: A hybrid whale optimization algorithm based on local search strategy for the permutation flow shop scheduling problem," *Future Gener. Comput. Syst.*, vol. 85, pp. 129–145, Aug. 2018.
[50] Z. Xuet, Y. Yu, H. Yachi, J. Ji, Y. Todo, and S. Gao, "A novel memetic whale optimization algorithm for optimization," in *Proc. Int. Conf. Swarm Intell.* Cham, Switzerland: Springer, 2018, pp. 384–396.

SOMNATH GANGULY received the Ph.D. degree from the Department of Electrical Engineering, Indian Institute of Technology (Indian School of Mines), Dhanbad, India, in 2021. He is currently an Assistant Professor with the Department of Electrical Engineering, Bankura Unnayani Institute of Engineering, Bankura, India. His research interests include electric power systems, renewable energy, grid energy storage, and soft computing technique.

JOYTI MUDI received the Ph.D. degree from the Department of Electrical Engineering, Indian Institute of Technology (Indian School of Mines), Dhanbad, India, in 2022. She is currently an Assistant Professor with the Department of Electrical Engineering, Bankura Unnayani Institute of Engineering, Bankura, India. Her research interests include power systems, alternative energy sources, power systems modeling, and power systems analysis.

VIVEKANANDA MUKHERJEE is currently an Associate Professor with the Department of Electrical Engineering, Indian Institute of Technology (Indian School of Mines), Dhanbad, India. He has more than 157 journal articles, six book chapters, and 38 conference proceedings. His Google citations total 6738, with an H-index of 46 and an i-10 index of 132. Stanford University ranks him in the top 2% of researchers. His research interest includes power system optimization.

TAPAS SI (Member, IEEE) received the B.Tech. degree in computer science and engineering from Maulana Abul Kalam Azad University (formerly the West Bengal University of Technology) and the M.Tech. degree in information technology and the Ph.D. degree in engineering from the National Institute of Technology Durgapur, West Bengal, India. He is currently an Associate Professor with the Department of Computer Science and Engineering, University of Engineering and Management, Jaipur, Rajasthan, India. He has published 75 papers in reputed international journals/conferences. His research interests include machine learning, swarm intelligence, medical image processing, and medical data mining. He is a member of the Institute of Engineers (India), the Soft Computing Research Society, and Machine Intelligence Research Labs, USA. He serves as a reviewer for journals of Springer, Elsevier, IEEE, and Nature. He is listed in Who's Who in the World® 2016 and 2020, Marquis Who's Who, USA.

SAURAV MALLIK (Member, IEEE) received the Ph.D. degree from the Department of Computer Science and Engineering, Jadavpur University, Kolkata, India, in 2017. His Ph.D. works were conducted with the Machine Intelligence Unit, Indian Statistical Institute, Kolkata, India. He was a Postdoctoral Fellow with the Department of School of Biomedical Informatics, The University of Texas Health Science Center at Houston, Houston, TX, USA, and the Division of Bio-Statistics, Department of Public Health Sciences, University of Miami Miller School of Medicine, Miami, FL, USA. He is currently a Postdoctoral Fellow in environmental epigenetics with the Harvard T. H. Chan School of Public Health, Boston, MA, USA. He has coauthored more than 75 research articles with a Google H-index of 17. His research interests include computational biology, bioinformatics, data mining, bio-statistics, machine learning, and pattern recognition. He was a recipient of the Research Associate of the Council of Scientific and Industrial Research, MHRD, Government of India, in 2017. He was a recipient of the Emerging Researcher in Bioinformatics Award from the Bioclues BIRD Award Steering Committee, India, in 2020. He is the editor of many journals.

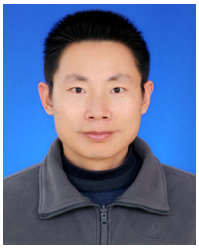

AIMIN LI was a Visiting Scientist with The University of Texas Health Science Center at Houston, USA, for 1.5 years. He is currently an Assistant Professor with the School of Computer Science and Engineering, Xi'an University of Technology, Shaanxi, China. He has more than 50 publications in different journals and conferences. His research interests include computational biology and machine learning.

AMAL AL-RASHEED received the Ph.D. degree in information systems from King Saud University, in 2017. She is currently an Associate Professor with the Department of Information Systems, College of Computer and Information Sciences, Princess Nourah bint Abdulrahman University (PNU), Riyadh, Saudi Arabia. She has been involved in many projects related to learning technologies, cyber security, and virtual reality. Her contributions in research projects in academia led to the publication of papers in many journals and conferences. Her research interests include education, knowledge management, data mining, data analytics, cyber security, and natural language processing. In 2017, she received the Research Excellence Award, by PNU, for her publications during performing the Ph.D. degree.

MOHAMED ABBAS received the B.Sc. degree in electronics engineering from the Faculty of Engineering, Mansoura University, Egypt, in 1998, and the M.Sc. and Ph.D. degrees in computer engineering from Mansoura University, in 2002 and 2008, respectively. Since this date, he has been an Assistant Professor with the College of Engineering, Department of Communications and Computer Engineering, Delta University. He is currently an Associate Professor with the Department of Electrical Engineering, King Khalid University, Abha, Saudi Arabia. His research interests include intelligent systems, medical informatics, nanotechnology, and bioinformatics.

AYMAN ABDULHAMMED received the B.Sc. degree in medicine from the Faculty of Medicine, Mansoura University, Egypt, in 2001. In 2010, he obtained the Egyptian Fellowship in clinical pathology. He is currently with the Biochemistry and Hormone Department, King Fahad Central Hospital, Gizan, Saudi Arabia. His research interests include clinical pathology, blood cancer, and biochemistry.